Paleoceanography and Paleoclimatology

RESEARCH ARTICLE
10.1029/2019PA003665

Intense Hurricane Activity Over the Past 1500 Years at South Andros Island, The Bahamas

E. J. Wallace[1], J. P. Donnelly[2], P. J. van Hengstum[3,4], C. Wiman[5], R. M. Sullivan[4,2], T. S. Winkler[4], N. E. d'Entremont[2], M. Toomey[6], and N. Albury[7]

[1]Massachusetts Institute of Technology/Woods Hole Oceanographic Institution Joint Program in Oceanography, Woods Hole, Massachusetts, USA, [2]Department of Geology and Geophysics, Woods Hole Oceanographic Institution, Woods Hole, Massachusetts, USA, [3]Department of Marine Sciences, Texas A&M University at Galveston, Galveston, Texas, USA, [4]Department of Oceanography, Texas A&M University, College Station, Texas, USA, [5]School of Earth and Sustainability, Northern Arizona University, Flagstaff, Arizona, USA, [6]U.S. Geological Survey, Florence Bascom Geoscience Center, Reston, Virginia, USA, [7]National Museum of The Bahamas, Nassau, The Bahamas

Key Points:
- Sediment cores from blue holes on Andros Island record intense hurricane activity over the past millennium and a half
- Multi-decadal shifts in Intertropical Convergence Zone position and volcanic activity modulate the hurricane patterns observed on Andros
- Hurricane patterns on Andros match patterns from the northeastern Gulf of Mexico but are anti-phased with patterns from New England

Supporting Information:
- Supporting Information S1

Correspondence to:
E. J. Wallace,
ejwallac@mit.edu

Citation:
Wallace, E. J., Donnelly, J. P., van Hengstum, P. J., Wiman, C., Sullivan, R. M., Winkler, T. S., et al. (2019). Intense hurricane activity over the past 1500 years at South Andros Island, The Bahamas. *Paleoceanography and Paleoclimatology*, *34*, 1761–1783. https://doi.org/10.1029/2019PA003665

Received 20 MAY 2019
Accepted 3 OCT 2019
Accepted article online 19 OCT 2019
Published online 27 NOV 2019

Abstract Hurricanes cause substantial loss of life and resources in coastal areas. Unfortunately, historical hurricane records are too short and incomplete to capture hurricane-climate interactions on multi-decadal and longer timescales. Coarse-grained, hurricane-induced deposits preserved in blue holes in the Caribbean can provide records of past hurricane activity extending back thousands of years. Here we present a high resolution record of intense hurricane events over the past 1500 years from a blue hole on South Andros Island on the Great Bahama Bank. This record is corroborated by shorter reconstructions from cores collected at two nearby blue holes. The record contains coarse-grained event deposits attributable to known historical hurricane strikes within age uncertainties. Over the past 1500 years, South Andros shows evidence of four active periods of hurricane activity. None of these active intervals occurred in the past 163 years. We suggest that Intertropical Convergence Zone position modulates hurricane activity on the island based on a correlation with Cariaco Basin titanium concentrations. An anomalous gap in activity on South Andros Island in the early 13th century corresponds to a period of increased volcanism. The patterns of hurricane activity reconstructed from South Andros Island closely match those from the northeastern Gulf of Mexico but are anti-phased with records from New England. We suggest that either changes in local environmental conditions (e.g., SSTs) or a northeastward shift in storm tracks can account for the increased activity in the western North Atlantic when the Gulf of Mexico and southeastern Caribbean are less active.

1. Introduction

In modern climate the North Atlantic basin experiences on average 12 named tropical cyclones per year (coast.noaa.gov/hurricanes, 2017). Many of these storms will either form in or pass through the warm waters of the Gulf of Mexico and Caribbean Sea on their way to the North American East Coast or Gulf Coast, putting coastal property and lives at risk. In 2017, Hurricanes Harvey, Irma, and Maria struck many Caribbean islands and locations along the U.S. coastline including Texas, Puerto Rico, and the Florida Keys. These three intense hurricanes killed thousands of people and caused approximately 215 billion USD in damage (Kishore et al., 2018; The hurricane season 2017: a cluster of extreme storms, n.d.). In 2018, Hurricanes Florence and Michael devastated portions of the U.S. coastline causing approximately 50 billion USD in damage and killing hundreds of people (https://www.ncdc.noaa.gov/billions/, 2019). Just this year (September 1, 2019), Hurricane Dorian made landfall in the northern Bahamas at Category 5 strength with sustained winds at 82 m/s and storm surge estimated at 7 m (www.nesdis.noaa.gov/content/hurricane-dorian-2019, 2019).

Despite the destructive nature of storms such as these, little is known about the forces that alter hurricane activity, particularly on multi-decadal to centennial timescales. One challenge is that the current observational record is short; Atlantic hurricane records maintained by the National Oceanic and Atmospheric Administration (NOAA) only extend back to 1851 CE and suffer from observation bias (Frappier et al., 2007; Landsea & Franklin, 2013). This relatively short and potentially incomplete dataset prevents a rigorous examination of the climate forcing mechanisms that influence storm activity on multi-decadal to centennial

timescales. This deficiency inhibits our ability to resolve hurricane/climate-interactions during climatic regimes not analogous to the short instrumental (and anthropogenically altered) period.

In the last decade, high-resolution sedimentary records of paleohurricane activity from coastal basins have been developed in an attempt to extend the hurricane record back in time (Denommee et al., 2014; Donnelly et al., 2015; Donnelly & Woodruff, 2007; Gischler et al., 2008; Lane et al., 2011; Lane & Donnelly, 2012; Toomey et al., 2013; van Hengstum et al., 2014). Strong winds, storm surge, currents, and waves generated by hurricanes displace and transport coarse grains such as shell fragments, sand, and gravel into depositional environments where finer grained sediments typically dominate. There, they form distinct layers of coarse material among the silt and/or clay that typically accumulate in these coastal basins, thereby providing a natural geological archive of past hurricane occurrence.

All of these reconstructions show periods of elevated hurricane activity interspersed by intervals of relative quiescence. Two records from the western coast of Florida (Mullet Pond (Lane et al., 2011); Spring Creek Pond (Brandon et al., 2013)) show marked variability in the frequency of high intensity events in the Gulf of Mexico. Lane et al. (2011) documented several active periods of intense hurricanes with the most active interval stretching from 2800 to 2300 years BP (years before present with present defined as 1950 CE by convention) with almost six intense events/century. Records from the Caribbean also show significant changes in hurricane frequency over the past millennium (Denommee et al., 2014; van Hengstum et al., 2014).

A growing number of paleohurricane reconstructions document the regional heterogeneity of past storm activity in the North Atlantic. In particular, records from the U.S. East Coast (Boldt et al., 2010; Donnelly et al., 2015; Mallinson et al., 2011) suggest heightened hurricane activity between 1400 and 1675 CE, while records from the Gulf of Mexico and Caribbean (Brandon et al., 2013; Denommee et al., 2014; Lane et al., 2011) suggest relatively low numbers of storms over this same period. These Gulf of Mexico and Caribbean records remain active up until the early 1400s while the U.S. East Coast records are quiet. This regional variability likely stems either from unfavorable local environmental conditions around the U.S. East Coast, from climate driven geographic variability in hurricane tracks and intensity, and/or random variability in hurricane paths. Using NCEP/NCAR Reanalysis data since 1948, Kossin (2017) illustrates the unfavorable local environmental conditions hypothesis by documenting periods in which vertical wind shear and sea surface temperature (SST) values in the Main Development Region (MDR) of the Atlantic were favorable for hurricane growth and survival while regional conditions along the U.S. East Coast were not. Other studies offer support for the second hypothesis suggesting that shifts in the positioning of the North Atlantic subtropical high (NASH) can dramatically change where hurricanes track (Elsner et al., 2000; Liu & Fearn, 1993). In particular, a more southwesterly position of the NASH might result in more straight moving hurricanes that track through the Caribbean Sea and make landfall in the Gulf of Mexico. Finally, the stochastic nature of hurricane landfalls makes it possible that the number of storms impacting a particular location might change from one sampled period to the next even if overall Atlantic hurricane activity remained stationary through time.

More paleohurricane records are needed from the Caribbean Sea to investigate the regional coherency of the existing records from the North American coastline or to identify any time transgressive shifts in hurricane activity across records. In addition, of the records we do have from the Caribbean (e,g., Donnelly & Woodruff, 2007; Toomey et al., 2013; van Hengstum et al., 2016), many have low sediment accumulation rates and high flooding thresholds, which result in rather low resolution records of only the highest magnitude events. A combination of undercounting in cores with low sedimentation rates (Woodruff et al., 2008) and the low occurrence rates of hurricanes in these records makes it difficult to distinguish between significant changes in hurricane tracks and random clustering of storm events at a particular location.

The ample accommodation space of relatively deep coastal karst depressions can result in systems with exceedingly high sedimentation rates where ambient fine-grained sediment fluxes are high. These basins are also often located in regions of the Atlantic prone to hurricane activity. In addition to the two published records of high-energy marine flooding events developed from a western Florida sinkhole (Lane et al., 2011) and a sinkhole on Abaco Island in The Bahamas (van Hengstum et al., 2016), there have been several records developed from coastal karst basins in the Caribbean Sea. Gischler et al. (2008) and Denommee et al. (2014) documented a 1500-year sedimentary archive of hurricane passages in the 125 m deep Lighthouse Reef Blue Hole, Belize. van Hengstum et al. (2014) further assessed the suitability of blue holes for hurricane

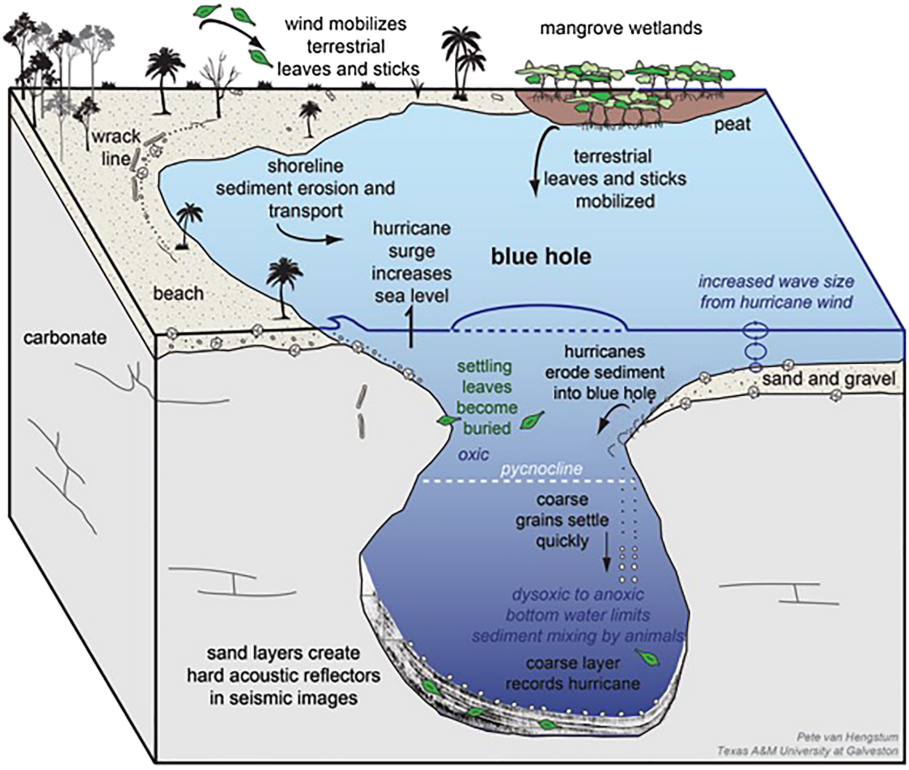

Figure 1. A conceptual model of the environment around the South Andros blue holes and the likely processes that create coarse-grained event beds at the bottom of the blue holes during storm events.

reconstructions and presented a sediment record of hurricane-induced event deposits from a blue hole on the Little Bahama Bank. Overall, deep coastal karst basins, like blue holes and sinkholes, provide several advantages for cyclone research: (i) after deposition, the sediments remain protected from ongoing wave action and coastal perturbations (e.g., other hurricanes) (Shinn et al., 1996); (ii) low benthic productivity, or even anoxia, limits bioturbation (Gischler et al., 2008); (iii) adjacent reefs, beaches, and/or flats provide abundant regional sediment supply (Gischler et al., 2008; Shinn et al., 1996); (iv) the basins provide accommodation space for sediments that is less dependent on sea level changes than other environments such as coastal wetlands or shallow lagoons (Dill, 1977); and (v) many coastal karst basins are not subject to complicating barrier beach dynamics (see Otvos, 2011).

Blue holes are water filled vertical openings that develop from the internal dissolution and cave development of carbonate banks and islands and subsequent ceiling collapse (Gischler et al., 2008; Gischler et al., 2013; Mylroie et al., 1995). Their high background sedimentation rates and wide distribution in hurricane prone regions make blue holes ideal candidates for increasing the spatial coverage of hurricane reconstructions. Background sedimentation in blue holes is typically clay- to silt-sized carbonate particles produced locally through inorganic precipitation in carbonate lagoons and peritidal flats (Milliman et al., 1993; Shinn et al., 1969). Coarse-grained gravel to sand layers in blue holes interbedded with allochthonous fine-grained carbonate clay and silt have been interpreted as high-energy deposits related to proximal hurricane passage (Denommee et al., 2014; Gischler et al., 2008; van Hengstum et al., 2014).

Similar to back-barrier environments, during a storm, currents and waves transport coarse-grained sediment from the surrounding reef flat or carbonate bank into the blue hole (Figure 1) (Gischler et al., 2008). Unlike back-barrier environments, the transported sediment can be sourced from all sides of the blue hole as well as from a collapse of the sediment slope on the rim of the hole (Brown et al., 2014). Since the blue hole is fully submerged, the transported sediment does not need to overtop a coastal barrier to leave a deposit. Instead, bottom currents need to be strong enough to suspend and transport larger grains over the hole. Once these grains are deposited in the hole, they cannot be reworked due to the ample accommodation space and large

water depths in many blue holes. In addition, the rate of sediment accumulation in blue holes is often much higher than back-barrier lagoons, because blue holes receive more fine-grained sediment under normal wave and tide conditions (Milliman et al., 1993). Additionally, it is unlikely that the sedimentary records contained in blue holes have been impacted by sea level driven shoreward barrier migration which has seriously affected the sensitivity of many back-barrier sites to storm overwash during the Holocene (Wallace et al., 2014).

Event beds identified in the modern facies of sediment cores from blue holes can be attributed to storms documented in the NOAA best track dataset (coast.noaa.gov/hurricanes, 2017) that passed close to the site of the core. For example, van Hengstum et al. (2014) found two coarse-grained event deposits in the instrumental period from Thatchpoint Bluehole on Abaco Island, The Bahamas. These event beds dated within uncertainties to Hurricane Floyd in 1999 and Hurricane Jeanne in 2004 that passed directly over Abaco.

In this study, we present three temporally overlapping high-resolution records of the frequency of event beds in blue holes from South Andros Island in The Bahamas. The longer reconstruction (AM4), spans the last 1500 years and is corroborated by results from shorter records (AM5 and AM2) from two nearby blue holes. The two most recently deposited event beds temporally correlate to the two most intense direct hurricane landfalls on South Andros (Unnamed 1919 and 1945 category 3 storms). The AM4 sediment record is one of the longest continuous cores collected from a blue hole to date (18 m) and is one of the best resolved records (in temporal resolution and length) of Atlantic paleohurricane activity. It is also well situated to assess the regional coherency of long-term hurricane activity from the Caribbean and U.S. coastline. We evaluate the temporal variability of hurricane activity on South Andros and the geographic patterns of hurricane activity along the U.S. East Coast, Gulf Coast, and the Caribbean over the past 1500 years by comparing this record to other reconstructions.

2. Study Sites and Methods

2.1. Study Sites

Andros Island is a carbonate island located on the Great Bahama Bank in the northeastern Caribbean (Figure 2). It is separated from the North American mainland by the Florida Strait to the northwest. This strait carries the Florida Current, the beginning of the Gulf Stream, the warm western boundary current that runs along the U.S. eastern coastline toward Newfoundland. The Great Bahama Bank is made up of horizontally bedded limestones of a shallow water marine origin (Mullins & Lynts, 1977; Spencer, 1967). The bank-top Holocene parasequence consists of carbonate sand, clay, and silt and living reefs with shallow marine, coral, and eolian limestone exposed in some sections. Andros Island is the largest of the Bahama islands and has at least 200 blue holes (Juberthie & Iliffe, 1994). It is made up of three main land areas, North Andros, Mangrove Cay, and South Andros, which are separated by tidal channels (Figure 2). The eastern margin of Andros is at a higher elevation and composed of sub-aerially exposed Pleistocene eolianite (Carew et al., 1998), while the western margin is dominated by tidal carbonate flats and algal marshes that are dissected by tidal channels (Black, 1933; Maloof & Grotzinger, 2012; Shinn et al., 1969). Radiocarbon dating of facies identified in cores suggests that the modern geomorphic setting of the marsh and tidal flats was established by 2000 years ago (Maloof & Grotzinger, 2012). The focus of our study is on cores taken from blue holes within the channels of the carbonate tidal flats on South Andros (Figure 2).

We collected cores (AM4 – N 23.78°, W 77.72°; AM2 – N 23.79°; W 77.65°; AM5 – N 23.77°, W 77.71°) from three different blue holes on the southwestern margin of South Andros Island in November 2014 (Figure 2). All three blue holes lie in tidal channels (<4 m in depth) within carbonate flats. Both red and black mangroves species grow on the tidal flats and algal marshes surrounding the blue holes. The sediments of the flats surrounding the blue holes are composed of unconsolidated carbonate mud that is mostly inorganically precipitated aragonite, with sand (>63 μm) to gravel (~25 mm) sized particles largely consisting of shell fragments (see Black, 1933; Milliman et al., 1993; Shinn et al., 1969). The most common fauna are gastropods, pelecypods, and foraminifera (Shinn et al., 1969).

The AM5, AM2, and AM4 blue holes are 150 m, 95 m, and 80 m in diameter, respectively, with maximum depths of 17 m, 18 m, and 95 m, respectively (Figure 2). Conductivity, temperature and depth (CTD)

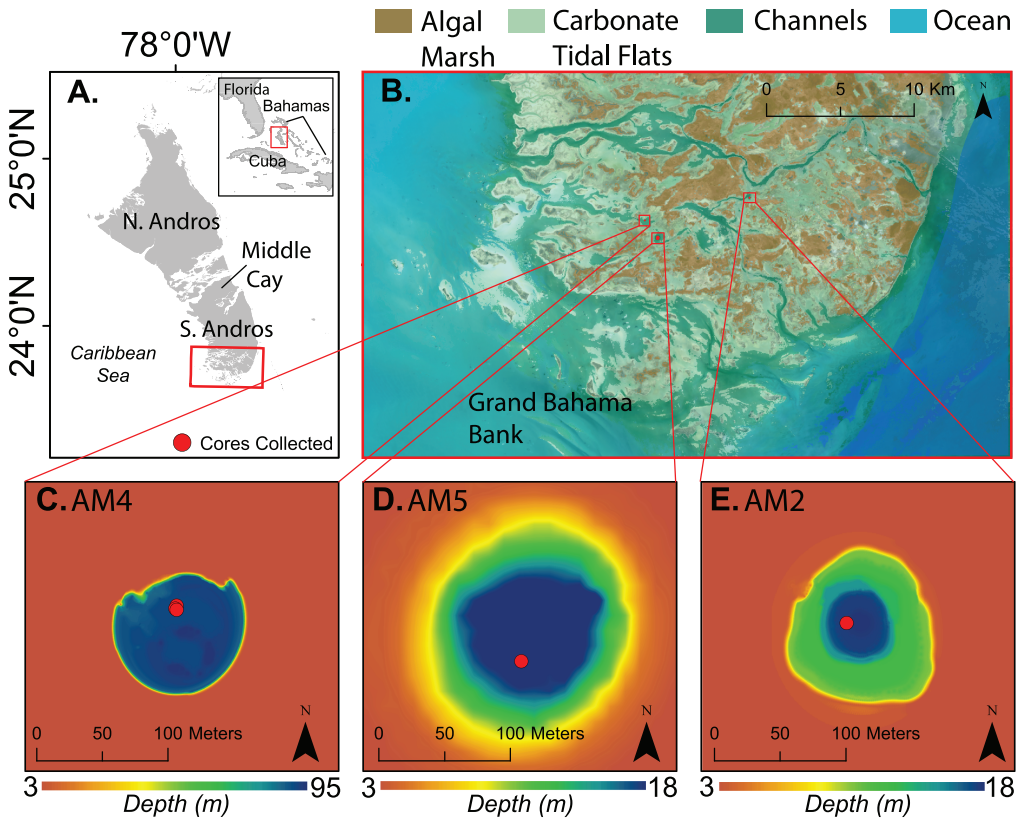

Figure 2. (A) Map of Andros Island, The Bahamas. **(B)** Blue hole locations on South Andros Island. The environment is characterized by algal marsh (brown) and carbonate tidal flats (light green) divided by tidal channels (teal) surrounded by ocean (blue). The bathymetry of each blue hole, **(C)** AM4 (N 23.78°, W 77.72°), **(D)** AM5 (N 23.77°, W 77.71°), and **(E)** AM2 (N 23.79°, W 77.65°), is shown. Note that the color bar range for panel C is different from D and E.

profiles for each of these circular basins indicates a halocline, below which the water in the blue hole is thermally and salinity stratified, and dissolved oxygen profiles show that the bottom conditions in each blue hole are dysoxic to anoxic (Figure S1).

Andros Island is positioned along the paths of many observed hurricanes that formed in the North Atlantic Ocean and Caribbean Sea. Since 1851 CE, 13 tropical storms and 7 hurricanes (category 1-5 on the Saffir-Simpson Scale) passed within 50 km of South Andros Island according to the NOAA best track dataset (coast.noaa.gov/hurricanes, 2017).

2.2. Field Methods

To assess the suitability of each field site as a coring location, we used an Edgetech 3100 Chirp sub-bottom sonar system to map sub-bottom stratigraphy, sweeping a bandwidth range from 4-24 kHz (Figure S2). These data, in combination with CTD profiles (Figure S1), allowed us to identify blue hole locations with a sizeable sediment package and where underwater caves connecting to the open ocean are unlikely.

Coring was carried out using a Rossfelder P-3 underwater vibracorer from a portable raft. We collected continuous vibracores from the blue holes: AM4 (~18 m in length), AM2 (~7 m) and AM5 (~8 m). In the case of the longer AM4 core, we failed to recover the sediment-water interface due to degassing of the sediment upon recovery and therefore, collected a short surface core from the same location using a clear polycarbonate tube with a core catcher to ensure that the sediment water interface was intact. The top 108 cm of the AM4 record is drawn from the replicate core where we carefully curated the core top. A comparison of the coarse fraction data from the longer drive and the replicate core indicate the point of overlap between the two sediment records (Figure S3).

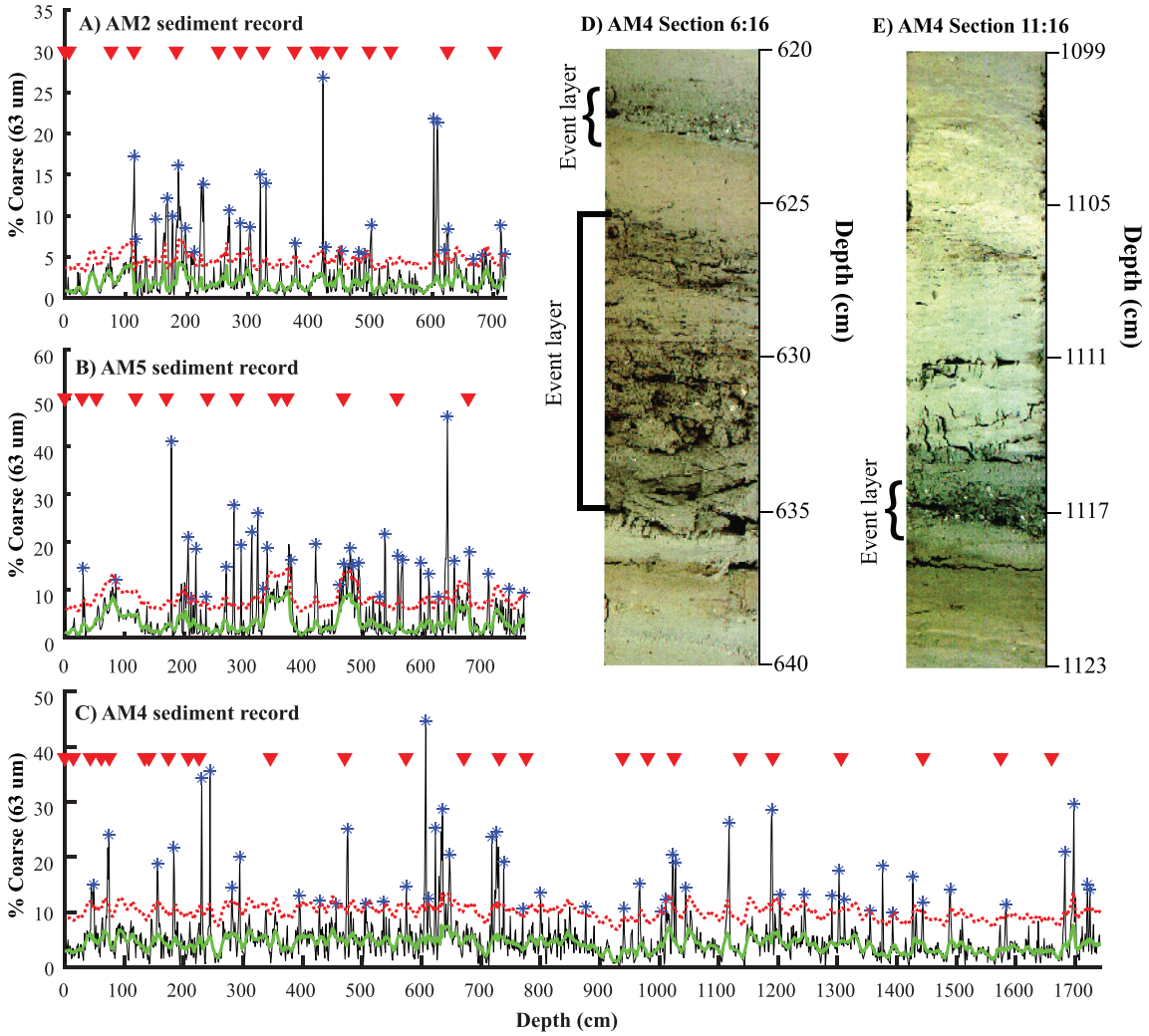

Figure 3. Percent sand fraction (>63 μm) vs. depth in core (black) from AM2 **(A)**, AM5 **(B)**, and AM4 **(C)** with a 10-point running mean filter (green) that excludes coarse fraction values above 10%. The red dashed line is the event cutoff threshold added to the filter. Events in each panel are denoted with a blue star. Location of ^{14}C dates are plotted as red triangles above the coarse fraction data. (**D)** Image from the sixth section of the AM4 sediment core from 622–640 cm in depth with two coarse-grained layers from 622–623 cm and 629–636 cm. (**E)** Image from the eleventh section of the AM4 sediment core from 1099–1123 cm in depth with a coarse-grained layer from 1113–1118 cm.

2.3. Sediment Analysis and Age Control

Following recovery, cores were sectioned and transported to the laboratory where they were split and described. In order to determine the percentage of coarse material, each core was sampled contiguously at 1-cm resolution. Samples of approximately 2 cm^3 were dried at 100 °C for 8 hours and then weighed to determine their dry mass. Each sample was wet sieved at 63 μm to retain the sand size, and greater, fraction and then dried to determine its 'coarse fraction' by dry weight (Figure 3).

Age constraints for the cores were derived from radiocarbon dating of terrestrial plant macrofossils. Mangrove leaves and plant matter preserved within the cores were dated at the National Ocean Science Accelerator Mass Spectrometer (NOSAMS) facility at Woods Hole Oceanographic Institution (WHOI). AM5, AM2, and AM4 have 15 dates over 780 cm, 17 dates over 720 cm, and 28 dates over 1761 cm, respectively (Table S1 and S2). The radiocarbon results were calibrated with IntCal13 (Reimer et al., 2013). Age models were developed using the Bayesian accumulation histories for deposits (BACON v 2.2) software (Blaauw & Christen, 2011). For the top of each core, age control was established using post-bomb radiocarbon dates with fraction modern values ($F^{14}C$) exceeding 1.000, meaning these samples were alive post-1950

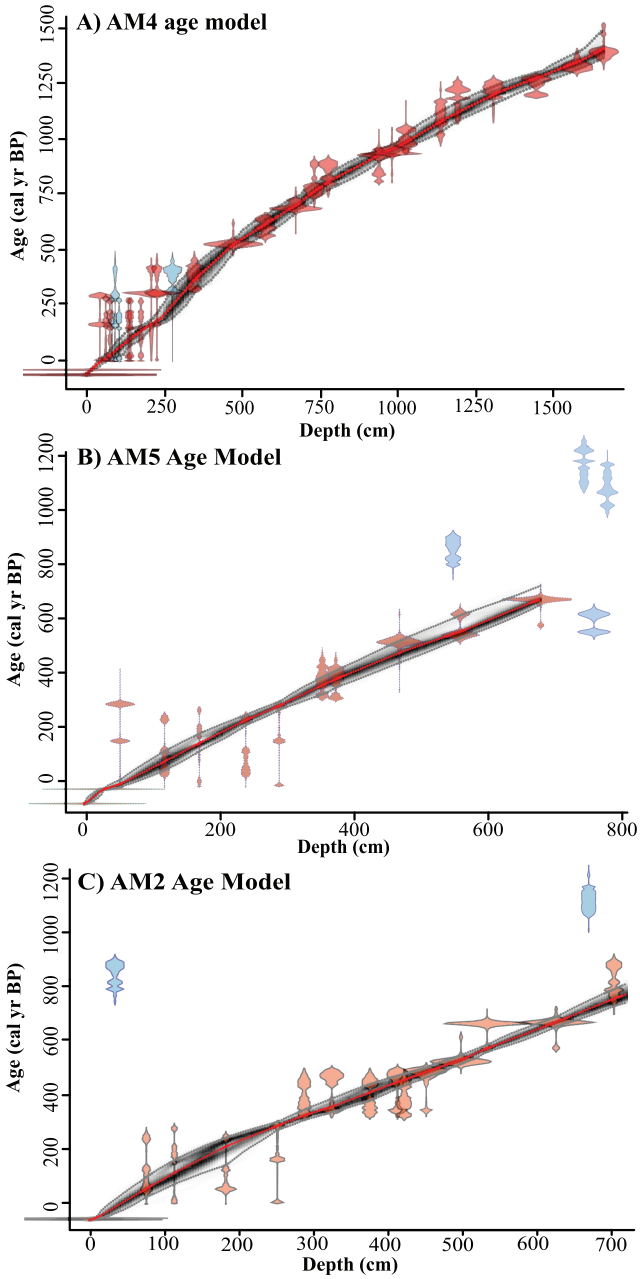

Figure 4. Age model (red dashed) derived from radiocarbon dates in Table S1 for AM4 **(A)**, AM5 **(B)** and AM2 **(C).** 95% confidence bounds are shaded in grey around the age model. Dates and age uncertainties used for the models are shown in pink. Post-bomb radiocarbon dates and a tie point setting the surface of each core to modern are also shown (pink horizontal bars). Rejected dates and age uncertainties are shown in blue. These figures were generated using BACON v2.2 age modeling software (Blaauw & Christen, 2011).

AD. These samples were calibrated with CALIbomb using the compiled Northern Hemisphere Zone 2 dataset (Hua et al., 2013).

Four radiocarbon samples were excluded from the age chronology of AM5 and two samples from AM2 as they lay outside the age depth ordering implied by the remainder of the dating evidence (Table S2 and Figure 4). In AM4, all 28 ages are in chrono-stratigraphic order. In the top of the record, there is a high density of dated samples with multiple possible calibrated age ranges, which results in abrupt changes in sedimentation rate in the Bayesian age-model analysis that are not correlated with event bed deposition. Therefore, we excluded four samples from the top 250 cm of the AM4 age model (Figure 4A). Removing these dates results in a near linear slope of the age model that matches the other 1700 cm of core and suggests a nearly constant sedimentation rate. The four samples omitted from the BACON age-model calculation contain calibrated ages ranges that date to within the 95% uncertainty bounds of the AM4 age model (Figure 4A).

2.4. Event threshold, Attribution and Frequency

We identified event beds in the cores based on visual inspection and using the coarse fraction data. The visible event beds were cross checked against the coarse fraction peaks identified as storms. Event beds in the South Andros sediment cores vary in appearance. Most event beds contain abrupt lower contacts, are light grey colored (Munsell color 2.5Y 6-1), contain visibly coarser grains, contain no sign of laminations, and range from one to fifteen centimeters in thickness. In a few cases, however, a coarse-grained event bed can only be distinguished visually by higher concentrations of mangrove leaf fragments. Event beds thicker than ten centimeters were reduced down to one centimeter in thickness for the age model as the event beds represent nearly instantaneous deposition.

In addition, we established an event bed cutoff in the coarse fraction data for each sediment core following the procedures of Donnelly et al. (2015). First, the coarse anomaly for each sediment core was calculated by subtracting a 10-point moving average from the coarse fraction data (Figure 3). This filter limits the influence of decadal variations in local background sedimentary processes while preserving coarse fraction peaks that are likely associated with short-lived storm events. We excluded coarse fraction peaks over 10% from this filter to prevent higher magnitude coarse fraction peaks from exerting a large influence on the filter and causing the exclusion of neighboring smaller peaks.

We define events as coarse anomaly peaks that exceed one sigma (68%) of the cumulative distribution of the coarse fraction data in the observational interval. The observational interval extends back to 1851 CE, the start of the best track dataset. The coarse fraction thresholds for AM4, AM2, and AM5 are 5.87%, 2.77%, and 4.94%, respectively (Figure 5).

Having established an event bed threshold and identified all the events in the records, we calculated an event frequency per century using the approach of Lane et al. (2011). This involved counting the number of events in a 100-year sliding window. This time window was chosen to allow for centennial scale comparisons in the record and to facilitate comparison with other records using century scale windowing (Figure 5). Event frequency plots using the 95% confidence bounds for the age of each event are included in the supplemental material (Figure S4). Results for 50-year sliding windows are also presented to allow for study of the multi-decadal variations in the record (Figure 6). To assess the sensitivity of the sites to

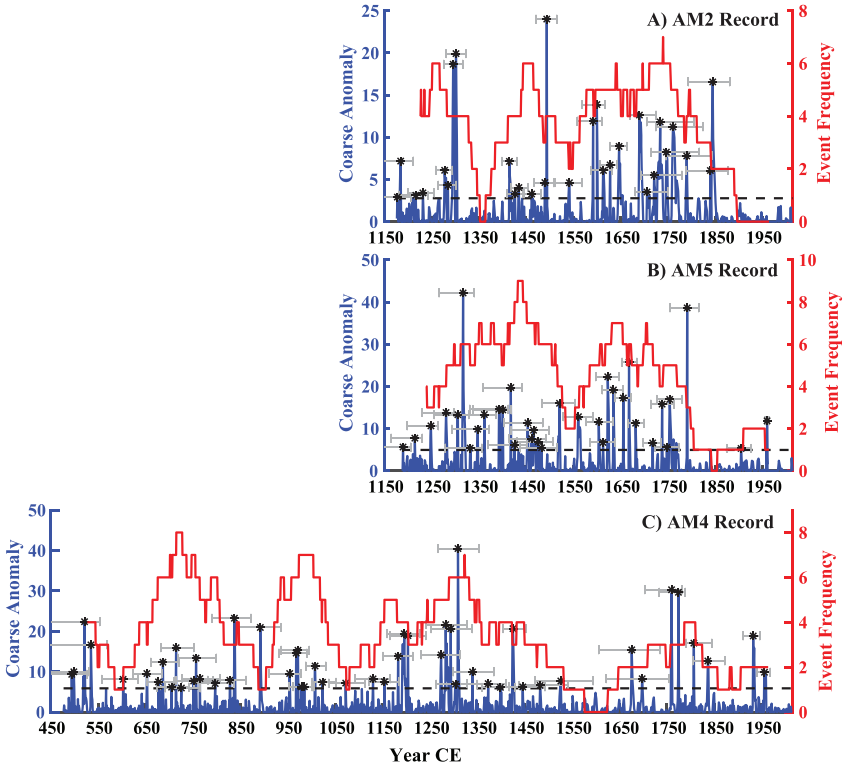

Figure 5. (A) Coarse anomaly plot (blue) for AM2 as a function of time derived from 15 radiocarbon dates. The dashed black line is the event bed threshold of 2.77%. **(B)** Coarse anomaly plot (blue) for AM5 as a function of time derived from 11 radiocarbon dates. The dashed black line is the event bed threshold of 4.94%. **(C)** Coarse anomaly plot (blue) for AM4 as a function of time derived from 17 radiocarbon dates. The dashed black line is the event bed threshold of 5.87%. Events in all panels are denoted as black stars. The 100-year moving window event frequency per century for each core is plotted in red. Grey error bars indicate 95% confidence bounds for the ages of each event.

hurricane induced deposition, we compared event deposits in the top sections of the core to observational storm data.

2.5. Calculating Expected Event Frequency

The number of storms hitting an island may vary as a result of changes in hurricane climate or random chance. Therefore, to determine the significance of changes in event frequency on South Andros, we calculated the cumulative Poisson probability (P) of the event frequency equaling or exceeding some value (k):

$$P(x,\lambda) = 1 - \sum_{k=0}^{k} \frac{\lambda^k e^{-\lambda}}{k!}$$

We calculated two estimates for the expected frequency (λ) for South Andros sites: 1) a site-specific estimate calculated using the frequency of category 3 or above hurricanes that passed within 50 km of the AM4 blue hole in the best track dataset (1851–2014), and 2) a regional estimate calculated using the methods described in the supplemental material. For the site-specific estimate, two storms passed within a 50-km radius at category 3 and above strength (coast.noaa.gov/hurricanes, 2017), resulting in an expected frequency of 1.23 events/century. For discussion of the site radius and storm intensity cutoff choices for the site-specific expected frequency calculation, see Section 4.1. The regional estimate results in an expected frequency of 2.12 events/century.

We determined active periods in the core using confidence intervals encompassing the expected random variability of hurricane strikes. Assuming event occurrence follows a Poisson process with a mean rate of 1.23 events/century for the site-specific estimate and 2.12 events/century for the regional estimate, we computed solutions for the 95th and 5th percentile (Ulm, 1990). For our AM4-specific estimate, these values are 3.86

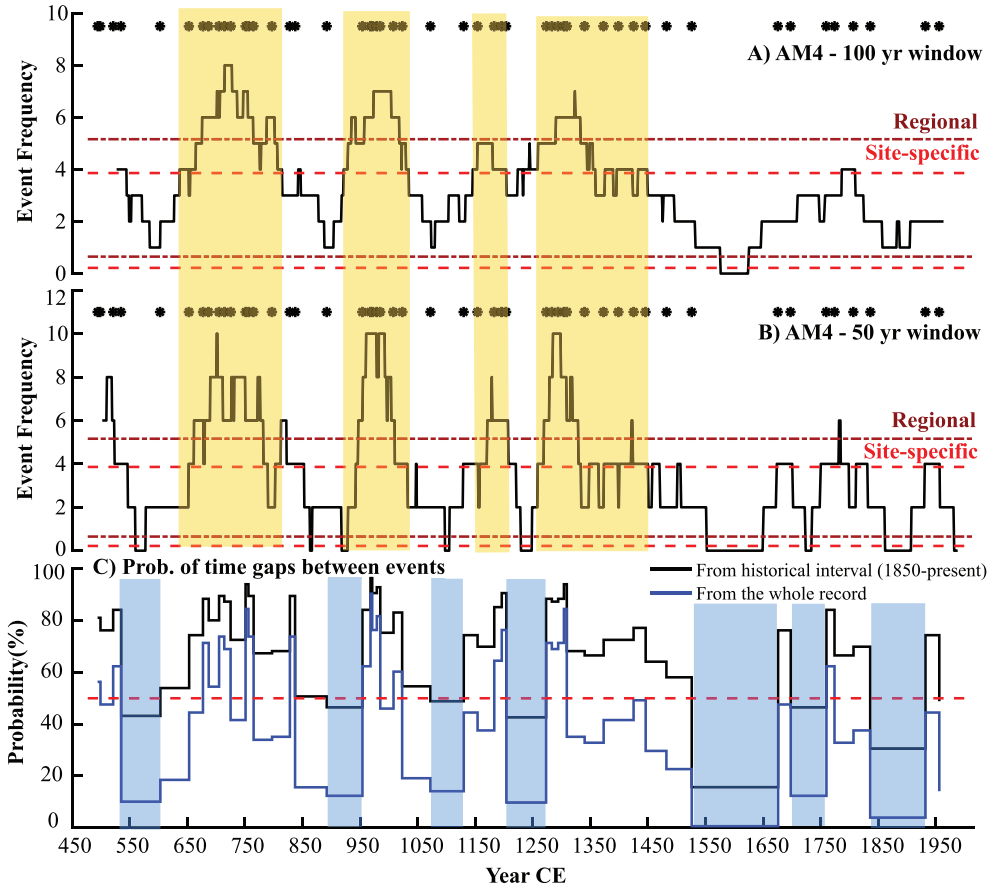

Figure 6. Event frequency per century for AM4 (black) with a 100-year sliding window **(A)** and a 50-year sliding window **(B)**. The probabilities of having no events over the time span between each event in the record **(C)**. The probabilities were calculated based on a recurrence interval of 81.5 over the observational interval (black) and 29 over the whole record (blue). Active and quiet intervals identified on South Andros are shaded in orange and blue, respectively. The dashed red lines are the site-specific and regional cutoffs for active and quiet intervals (3.86 and 0.22 events/century and 5.16 and 0.65 events/century respectively). The timing of each event identified in AM4 is denoted by the black stars above each panel.

and 0.22 events/century, respectively, and for our regional estimate, they are 5.16 and 0.65 events/century, respectively (Figure 6 and Table S3). Over the observational period, fewer storms on average have passed by South Andros than other regions in the Caribbean included in our regional estimate (coast.noaa.gov/hurricanes, 2017). Thus, our regional estimate, which applies to the entire northern Caribbean, overestimates the random variability in storm tracks on South Andros where there have been fewer storms on average. Therefore, we define active periods on South Andros Island using the site-specific estimates but still show the regional estimate cutoffs in Figure 6. 'Active periods' were characterized as time intervals when the 100-year window event frequency exceeded each site's specific threshold.

To define significant quiet intervals, we calculated the probability of having each time gap between event beds in the record. The probability of having no events (P_T) for r number of years between each event in the record is:

$$P_T = \left(1 - {}^{1}/_{T}\right)^{r}$$

The recurrence interval (T) was set at 81.5 year/event based on the two intense hurricanes that passed the AM4 blue hole over the length of best track dataset (163 years). Time gaps between events in the record where the probability of having no events over this length of time (P_T) was below 50% are characterized as quiet intervals. We also calculated the same probability using a recurrence interval spanning over all events in the record (29 year/event) for comparison (Figure 6).

3. Results

3.1. Event Bed Description

On visual inspection, sediment cores from all three blue holes have similar lithofacies: light grey (Munsell color 2.5Y 6-1) colored sediment with tan (Munsell color 2.5Y 7-4) and white (Munsell color 2.5Y 8-1) laminations. The sediment is predominantly fine-grained carbonate with occasional very-fine gravel (2-4 mm) to medium sand (0.25-0.5 mm) layers (Figure 3D and 3E). There is no evidence of bioturbation.

Both the AM2 and AM4 sediment cores exhibit a reduced rate of sediment accumulation moving up-core (past to present). AM2 starts with a sedimentation rate of 1.0 cm/yr for first 530 cm of the core then decreases to 0.7 cm/yr for the top 185 cm (Figure 4C). AM4 starts with a sedimentation rate of 1.4 cm/yr for the bottom approximately 1100 cm of the core and decreases to ~ 0.9 cm/yr for top 600 cm of the core (Figure 4A). The AM5 record, on the other hand, maintains a nearly uniform sedimentation rate of 1.0 cm/yr over the entire 771 cm length of the core (Figure 4B). All three records are near annually-resolved such that on average a one cm sample represents close to one year's worth of sedimentation.

The coarse fraction of event beds in the South Andros cores ranges from 6 to 40% sand sized (>63 μm) or larger particles. Many event beds contain white shell fragments (~2 mm) and concentrated amounts of mangrove leaf fragments. Some event beds are topped with higher concentration of the mangrove leaves while other event beds have leaf fragments scattered throughout the layer. Since the late 5th century CE, AM4 has recorded 51 events (Figure 5C). While AM5 extends back only to about 1190 CE, it captures 34 events (Figure 5B). The AM2 record captured fewer events than AM5 with only 29 events observed since about 1175 CE (Figure 5A). Both AM4 and AM5 document only two coarse-grained event deposits that date post-1851 CE (Figure 5). The resultant average event frequencies for the time period of overlap (1190 CE–present) in AM4, AM5, and AM2 are 2.98, 4.49, and 3.72 events/century, respectively.

3.2. Changing Event Frequency

Over the past 1500 years, all three records show evidence of active and quiescent periods of event frequency spanning a century or more. Looking at the 100-year window event frequency, AM4 exhibits four active intervals from approximately 640 to 815 CE, 920 to 1035 CE, 1145 to 1205 CE, and 1300 to 1450 CE (Figure 6A). The time interval with the most activity was from 640 to 815 CE at 6.3 events/century, almost double that of the average event frequency for the entire record. Using the site-specific expected frequency (λ), the probability of exceeding 5 events/century is 0.17%. Compared to the modern event frequency on South Andros, these active intervals exceed what would be expected based on the random nature of hurricane occurrence (>3.86 events/century- the 90% confidence interval). The 50-year window event frequency emphasizes periods of extremely high activity, namely from 690 to 710 CE, 960 to 990 CE and 1280 to 1300 CE. During these periods, using the 50-year moving window, the frequency of storm occurrence exceeds nine events per century with a probability of 7.0×10^{-5} %.

We define seven quiet intervals in the record in which the cores record zero event beds and the probability of having zero events over each time interval is below 50%. These quiet intervals range from 535 to 600 CE, 890 to 955 CE, 1070 to 1130 CE, 1205 to 1270 CE, 1530 to 1680 CE, 1700 to 1760 and 1840 to 1930 CE (Figure 6C). Of these intervals, the quietest periods occur later in the record. In particular, the probability of having 150 years of sustained inactivity from 1530 to 1680 CE is only 16% given the recurrence interval of hurricane events throughout the record.

4. Discussion

4.1. Potential Influence of Changing Sea Level

Large sea-level changes could greatly impact the susceptibility of the AM4, AM2, and AM5 blue holes to hurricane-induced event deposits by changing their depositional environment. The South Andros blue holes most likely formed during sea level oscillations in the Quaternary (Mylroie et al., 1995; Peltier & Fairbanks, 2006). During the Holocene (12 kyr BP to present), the environmental conditions in these basins changed in response to relative sea-level rise. Sea-level curves from the Caribbean (Fairbanks, 1989; Hubbard et al., 2005; Khan et al., 2017; Milne & Peros, 2013; Toscano & Macintyre, 2003) suggest rapid sea-level rise (~5 mm/yr) up until 8 kyr BP, with slower rates between 8 kyr BP and 4 kyr BP, and leveling off to a stable rise of ~0.4 mm/yr over the past 3000 years. With sea-level rise, the blue holes on South Andros transitioned

from sinkholes in a subaerial landscape to marine dominated conditions in tidal carbonate flats (Gischler et al., 2013; Gregory et al., 2017; van Hengstum et al., 2016). None of the cores from South Andros blue holes penetrated deep enough to recover the facies associated with terrestrial sinkhole environments (i.e., algal sapropel, lacustrine marl). In addition, all three cores do not show meaningful changes in sedimentation rate (Figure 4). This suggests that the tidal and wave environment in and around these blue holes has not changed significantly over the past 1500 years.

The depositional environment around South Andros has likely also remained stable over the past 1500 years. The tide dominated coasts of Andros allow tidal flats to remain open to the sea and experience unrestricted tidal flushing and freshwater flows (Maloof & Grotzinger, 2012). This provides the perfect environment for expansive development and growth of mangroves (Mckee et al., 2007; Ramcharan & McAndrews, 2006). The presence of mangrove leaves and plant matter throughout the length of our cores suggest that intertidal carbonate flats and algal marshes have consistently surrounded our blue holes over the past 1500 years. In addition, a recent study of a tidal carbonate flat in northwest Andros suggests that the tidal channels in this environment predominantly remained stationary over the past 1200 years (Maloof & Grotzinger, 2012). Taken together, the modest sea-level change over the last 1500 years (~60 cm given the recent rise at 0.4 mm/yr), the stable sedimentation rates found in the cores, and the consistency of the macro flora throughout the length of the cores suggest relative geomorphic stability on South Andros over the time period of study.

4.2. Modern Event Calibration

Event beds in the cores are likely a result of predominantly coarse-grained sediment transport from the surrounding tidal carbonate flats into the holes during high-energy wave and storm surge events. In the shallow coastal waters around South Andros, both waves and currents are important to sediment transport (Black, 1933; Bourrouilh-Le Jan, 2007; Shinn et al., 1969). During minor storms and the waxing and waning stages of more intense storms, elevated current velocities in tidal channels create strong bottom shear stress values and bottom currents, which transport fine-grained sediment. There is well documented evidence for off-bank export of fine sediments in The Bahamas (Boardman & Neumann, 1984; Gischler et al., 2008; Kier & Pilkey, 1971; Pilskaln et al., 1989; Shinn et al., 1993; Wilber et al., 1990). This leads to winnowing of fines in tidal channels, leaving behind a coarse-grained sediment source that can be mobilized during severe storms.

During a severe storm, (i.e., intense hurricane), high winds and waves at the site create currents and storm surge (Figure 1), raising water levels and inundating the intertidal and supratidal zones (Black, 1933; Bourrouilh-Le Jan, 2007). Thus, during the height of intense hurricanes, sediment transport is likely no longer restricted to tidal channels. The surface wave and current activity during these storms increases bottom shear stress around the blue holes and transports coarse sediment into the blue hole after a critical bottom shear stress threshold is crossed (Miller et al., 1977). The heavier grains settle to the bottom of the blue hole first followed by lighter particles (Brown et al., 2014; Maiklem, 1968) and mangrove fragments.

At least fourteen hurricanes passed within 100 km of South Andros since 1851 CE (Figure 7), but many of these were likely locally too weak to instigate event-bed deposition in the blue holes or had offshore directed maximum winds that can inhibit event-bed deposition. While an array of storm characteristics combines to influence local conditions, typically the proximal passage of intense storms is required to deposit event beds (Brandon et al., 2013; Donnelly et al., 2015; Lin et al., 2014; Woodruff et al., 2008). In the case of hurricanes leaving deposits in coastal sinkholes in Apalachee Bay, Florida, hydrodynamic modeling of a large suite of downscaled hurricane simulations revealed that a wide range of different storm characteristics (e.g., intensity, track, and size) could produce large enough storm surges to overtop the coastal barrier and leave a sediment record at the site. However, the vast majority of storms that actually left a deposit at the site were nearby landfalls of category 3 or greater intensity (Lin et al., 2014). We expect similar local intensity threshold type of behavior to be operating in blue hole settings.

In the case of AM4 and AM5, only two coarse-grained event beds were deposited over the last 163 years. Our Bayesian age model (at 2σ) from AM4 (Figure 4A) indicates that the upper most event bed (event bed 1: 44–50 cm) dates between 1944 and 1973 CE (with a median age of 1958). According to the best track data, only two hurricanes passed within 100 km of the site between 1944 and 1973, and both occurred in 1945. Both storms made direct landfall on South Andros (Figure 7). The first struck South Andros from the southeast

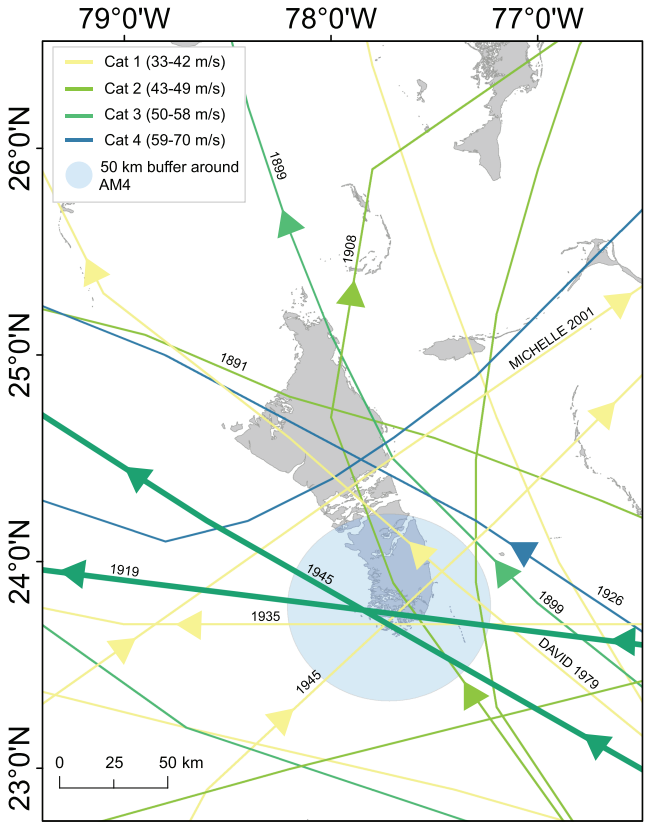

Figure 7. Historical hurricane tracks (1850–present) passing within 100 km of the AM4 blue hole on South Andros Island (N 23.78°, W 77.71°). In bold are the two storms (1945 and 1919) that left a deposit in the South Andros blue holes.

on September 15 as it transitioned from category 3 to category 4 intensity with sustained winds of approximately 58 m/s en route to a landfall in Miami, Florida six hours later. The second hurricane to strike South Andros in 1945 occurred on October 12 as a category 1 storm with sustained winds of ~41 m/s. This storm approached South Andros from the southwest (Figure 7; coast.noaa.gov/hurricanes, 2017).

The two calibrated radiocarbon samples (Table S1 and Figure 3) from above and below this event bed constrain the age of emplacement to between 1936 and 1950 CE. The sample from one centimeter above the first event bed yields three calibrated age ranges: 1648–1669 CE (prob. 0.52), 1781–1798 CE (prob. 0.45), and 1946–1950 CE (prob. 0.029). The sample below the event bed has four calibrated age ranges: 1663–1682 CE (prob. 0.23), 1737–1757 CE (prob. 0.11), 1761–1804 CE (prob. 0.46), and 1936–1950 CE (prob. 0.20). Only the youngest calibration for each sample are both in stratigraphic order and intersect with the Bayesian age model (Figure 4A). Thus, considering only the youngest age range from the radiocarbon results for these two samples, event bed 1 was deposited as early as 1936 CE and no later than 1950 CE. Other than the two 1945 storms, there were no other storms passing close by South Andros over this time span. We attribute event bed 1 to the more intense September 15 landfall; however, we cannot rule out the less intense landfall 27 days later from also contributing to the deposit.

A small peak in coarse fraction between 62 and 64 cm in AM4 that does not make our statistical detection threshold dates to between 1924 and 1956 CE (with a median age of 1943) in our age model. Four events impacted South Andros in this interval. Since we have attributed the first event layer to one of the 1945 storms, we are left with two other storms. The first is a category 4 storm that passed approximately 70 km to the northeast of the AM4 blue hole on September 17, 1926. The second storm was the infamous Labor Day Hurricane of 1935, which made direct landfall at South Andros as a category 1 storm with sustained winds of 36 m/s (Figure 7). Assuming that this small peak in coarse fraction is the result of one of these two hurricanes, the fact that a direct strike category 1 and/or a more distal passage of a category 4 hurricane were not able to leave a deposit that meets our detection threshold suggests that the majority of event beds that exceed our detection limit are deposited by direct strikes of intense hurricanes.

This assessment is further supported by the fact that no event beds are present that date to the relatively close passage (within 75 km) of two category 1 hurricanes in 2001 (Michelle) and 1979 (David) or the passage of the 1908 (category 2), 1899 (category 3), and 1896 (category 2) hurricanes east of our study sites (Figure 7). The lack of the event bed in AM4 from Hurricane Michelle in 2001 is supported by a study presenting observations from Andros Island post-hurricane (Rankey et al., 2004). Rankey and others found minimal impact on shorelines or tidal flats in the aftermath of Michelle, which suggests that it was too weak to create major geomorphic changes on the island.

The second event bed in AM4 that exceeds our detection threshold (event bed 2: 72–75 cm) dates to between 1910 and 1946 CE (median age 1932) based on our age model. Five hurricanes are potential candidates for this event bed: the two 1945 storms, the 1926 and 1935 hurricanes discussed above, and a category 3 hurricane in 1919. This 1919 hurricane directly struck South Andros on September 8, 1919 with sustained winds of ~53 m/s (Figure 7; coast.noaa.gov/hurricanes, 2017). Given the uncertainty of the current age model, we are unable to eliminate the category 1 storm in 1935 or the category 4 1926 hurricane that passed 70 km to the northeast as possibly depositing event bed 2. However, we provisionally attribute this event bed to the direct landfall of the 1919 storm. This interpretation is supported by the fact that other hurricanes of similar character to the 1935 and 1926 events (the 2001, 1979, 1899, and 1896 hurricanes mentioned above) failed to leave a detectable event bed in AM4. Given our assessment of the historical storms that both left an event bed

and failed to leave a discernible deposit, we infer that the AM4 sedimentary archive is generally capturing intense hurricanes (>category 3) passing within approximately 50 km of the site. However, we do acknowledge that this is a rough estimate given the uncertainty associated with estimates of maximum wind speeds for the best track dataset and the lack of reliable radius of maximum wind data for these earlier storms. In addition, we also note that it is conceivable that certain combinations of storm characteristics (e.g., size, translational velocity, intensity, track) could result in some lower intensity storms leaving a deposit at the site (Lin et al., 2014). Future work on hydrodynamic modeling of hurricanes over carbonate tidal flats is needed to better constrain what storm characteristics are important for leaving deposits in blue holes.

The AM5 core also contains two event beds that were deposited during the interval covered by the best track data. The uppermost event bed dates to 1952 ± 10 CE and the second one dates to 1894 ± 30 CE. These event beds are also consistent with deposition associated with the 1945 and 1919 category 3 hurricane strikes. The AM2 reconstruction, in contrast, contained no event beds over the last 160 years of deposition and thus lacks any modern analog. The AM2 blue hole is located about 7 km east of the AM4 and AM5 blue holes which places it closer to the protective sub-aerially exposed bedrock portion of the eastern margin of South Andros (Figure 2). This location may have sheltered it from the most extreme hydrodynamic conditions attendant with the 1945 and 1919 hurricanes.

4.3. South Andros Site Comparison

While all three blue holes on South Andros are located in the same depositional environment, they have slightly different settings and are thus subject to somewhat different sediment sources and transport pathways. The AM2 blue hole is both farther inland and closer to the eastern side of the island compared to the AM4 and AM5 blue holes. It is also located directly on a large tidal channel which does not directly connect to the larger channel containing the AM4 and AM5 blue holes (Figure 2). It is possible that the AM2 blue hole's different, more inland, location within the carbonate tidal flat environment makes it susceptible to a different population of landfalling storms (e.g., intensity, duration, track, size). This might explain why it does not record the two most recent category 3 events passing over South Andros (1945 and 1919). In addition, this might also explain a gap in activity from 1302-1415 CE observed only in AM2 (Figure 5). Overall, AM2 still shows similar event frequency patterns (Figure 5) as AM4 and AM5. Like both AM5 and AM4, AM2 shows heightened hurricane activity from 1575 to 1800 CE and 1400 to 1475 CE.

The AM5 record corroborates the results from AM4 (Figure 5). Located 1.5 km south-southeast of the AM4 blue hole in the same tidal channel (Figure 2), AM5 also exhibits similar active and quiescent periods showing high hurricane numbers from approximately 1600 to 1800 CE and 1300 to 1500 CE and low hurricane frequency from 1500 to 1580 CE and 1820 CE to the present. Both records document a decrease in hurricane activity in early 13th century. However, the overall frequency of event bed deposition at AM5 is higher than at AM4, recording approximately one additional event per century throughout the entire record. This could be a result of the AM5 blue hole's increased exposure to currents within the tidal flat system. The AM5 blue hole is located in a channel between carbonate tidal flats (Figure 2), whereas the AM4 blue hole is more sheltered and located directly offshore a small supratidal algal marsh (~80 m away). Both the AM2 and AM5 sediment records confirm the overall temporal variability observed in AM4 within age uncertainties, thus we use the longer and better dated AM4 reconstruction when discussing hurricane frequency changes on South Andros Island.

4.4. Climatic Forcing of Hurricane Activity on South Andros Island

Our high-resolution record from South Andros Island indicates dynamic patterns of intense hurricane activity over the past millennium. Much like other reconstructions of hurricane activity from the North Atlantic including Blackwood Sinkhole (van Hengstum et al., 2016), Laguna Playa Grande in Puerto Rico (Donnelly & Woodruff, 2007), and Salt Pond in Massachusetts (Donnelly et al., 2015), there are pronounced active and quiet intervals of intense hurricane strikes on South Andros. Given that these active intervals lie outside our 90% confidence intervals encompassing the random variability of hurricane strikes (Section 2.5), these variations in hurricane activity are likely due at least in part to the complex interactions of climate variables over this time period. Our sedimentary archive sheds light on some climate mechanisms controlling hurricane variability on longer time scales.

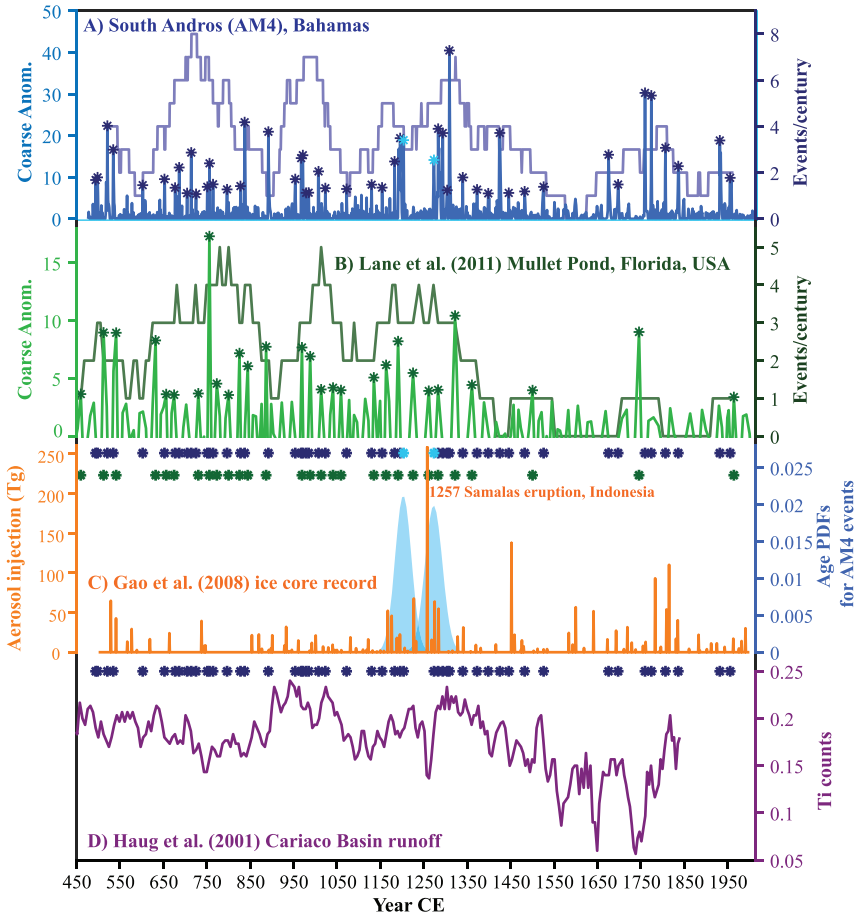

Figure 8. Comparison of hurricane proxy records from the Atlantic basin. **(A)** Coarse anomaly plot (blue) for AM4 as a function of time. Events are denoted as dark blue stars. The 100-year moving window event frequency per century is plotted in dark blue. **(B)** Coarse anomaly plot (green) for Mullet Pond, FL (Lane et al., 2011) as a function of time. Events are denoted as dark green stars. The 100-year moving window event frequency per century is plotted in dark green. **(C)** Annual stratospheric volcanic sulfate aerosol injection for the past 1500 years from ice core records (Gao et al., 2008). Blue probability distributions depict the age uncertainty for the two hurricane events (light blue stars) on either side of the 70-year gap in activity during the early 13th century. The timing of South Andros (dark blue stars) and Mullet Pond (dark green stars) events are plotted above the data. **(D)** Ti record from the Cariaco Basin reflecting changes in terrestrial runoff and the position of the ITCZ (Haug et al., 2001).

A recently published lower resolution hurricane reconstruction from Blackwood Sinkhole on Abaco Island in The Bahamas (van Hengstum et al., 2016) suggests that the Intertropical Convergence Zone (ITCZ) position modulates paleohurricane activity in the Caribbean. A more northerly position of the ITCZ decreases vertical wind shear in the Atlantic Main Development Region (MDR) favoring cyclogenesis and thus, increasing the likelihood of intense hurricane landfalls (Kossin et al., 2010; Kossin & Vimont, 2007; Schneider et al., 2014).

The Abaco Island record shows decreased hurricane activity from 1000 to 1500 CE, which was attributed to a southward shift in the ITCZ. In contrast, the record from South Andros Island shows increased numbers of intense hurricanes in The Bahamas over this time span (1145–1205 CE and 1300–1450 CE) (Figure 8). The dramatically different resolutions, sensitivities, and timescales of the South Andros and Abaco records make comparing their hurricane histories and potential climatic forcing difficult (Figure S5). For example, only ten events are recorded at Blackwood over the last 1500 years while fifty-one events are recorded at South Andros. The Blackwood Sinkhole record is valuable for looking at the connections between the landfalls of the highest intensity hurricanes and the ITCZ on multi-centennial timescales. However, the lower resolution of the Blackwood record compared with our blue hole sites, prevents direct comparisons.

While caution should be exercised in using only a single reconstruction to infer climatically meaningful patterns, here we explore the potential role of subtle multi-decadal shifts in the ITCZ on Caribbean hurricane activity by comparing the AM4 reconstruction with the similarly resolved Cariaco Basin Ti record (Haug et al., 2001). The position of the ITCZ is generally thought to have shifted southward over most of the Holocene (Schneider et al., 2014). Superimposed on this Holocene trend are more moderate but abrupt shifts in the ITCZ position over the past 2000 years as indicated by the Cariaco Basin Ti record (Haug et al., 2001). Many of these multi-decadal to centennial scale shifts correspond to times of changes in hurricane activity on South Andros. Throughout most of the record, increased hurricane activity on South Andros corresponds to local maxima in Cariaco Basin Ti counts (Figure 8D) and thus, a more northerly position of the ITCZ. This includes active intervals from 920 to 1035 CE, 1145 to 1205 CE, and 1300 to 1450 CE as well as increased numbers of events from the mid-16th century to the mid-17th century. Similarly, the largest gap in hurricane activity on South Andros (1530–1680 CE) occurred during the Little Ice Age when there were cooler SSTs in the North Atlantic (Mann et al., 1999; Richey et al., 2009) and the ITCZ had moved southward (minimum in Ti counts) (Figure 8D). However, this trend does not apply during the earliest active interval on South Andros from 640 to 815 CE when the ITCZ is inferred to be in a southerly position (Cariaco Basin Ti counts at a local minimum) (Figure 8D).

For most of the last 1500 years, we reconstruct multi-decadal scale changes in intense hurricane activity on South Andros occurring simultaneously with multi-decadal changes in ITCZ position (Figure 8). In general, when the position of the ITCZ is more northerly, we see increased storm activity in our cores from South Andros Island. Only in the first 400 years of the record (640–815 CE) do we observe high hurricane activity with little change in ITCZ position. More highly resolved tropical cyclone reconstructions are needed from across the western North Atlantic (and globally) to better assess the connection between ITCZ position and tropical cyclone variability on multi-decadal time scales.

In the time span between the two most recent active intervals, South Andros experienced an unusual quiet interval from 1204 to 1273 CE. This multi-decadal scale gap in activity is most clearly shown in the 50-year window event frequency but is smoothed out in the 100-year window frequency (Figure 6). Over this 69-year period, there were no hurricane strikes recorded in the sediment record (Figure 8). Based on the recurrence interval of hurricanes over the past 163 years, there is a 43% likelihood of seeing a gap in storm activity of this size. It is even less likely (10%) if we calculate our recurrence interval based on the entirety of the record (Figure 6).

Age-model uncertainties in the AM2 and AM5 records make it difficult to assess whether these cores show a similar gap in activity over this same time period. While both records show less activity occurring over this time span, they do not observe a complete lack of event beds like AM4. Both AM2 and AM5 contain two event beds from 1204 to 1273 CE (Figure 5). However, both AM2 and AM5 also have much higher age uncertainties than AM4 (Figure 4). The end of the AM5 core, encompassing this time interval, shows the largest uncertainty in its age model containing four dates which were out of stratigraphic order and excluded from the age model (Figure 4B). Given the dating uncertainty in these two nearby records, we will continue to assess this gap in activity using the timing constrained by the AM4 age model.

Interestingly, over this same time period within the AM4 age-model uncertainties, ice cores from Greenland (Gao et al., 2008) and Antarctica (Sigl et al., 2014) record increased sulfate aerosol loading in the atmosphere indicative of abundant volcanic eruptions (Figure 8C). Indeed, the strongest eruption on record in these cores was the Samalas Volcano in Indonesia in 1257 (Gao et al., 2008). Cooling of the ocean surface (Hansen et al., 2005) and subsurface (Church et al., 2005) associated with aerosols from volcanic activity can cause short term reductions (1-3 years) in tropical cyclone intensity (Evan, 2012; Korty et al., 2012), but very little is known about longer timescale impacts. Surface ocean heat content plays an important role in hurricane formation and growth. Typically, hurricanes require localized warm SST to provide energy to the storm and only develop over ocean water with surface temperature exceeding 26°C (Emanuel, 2003; Gray, 1998; Wallace et al., 2014). Perhaps the rapid introduction of aerosols to the atmosphere beginning around the mid-12th century and continuing across the span of this anomalous quiet period in hurricane activity cooled the ocean surface in the MDR and/or locally in The Bahamas enough to reduce the number of high intensity storms in the Atlantic that could leave a deposit at sites like the AM4 blue hole. Records from Iceland (Sicre et al., 2008) and the Cariaco Basin (Haug et al., 2001) suggest that climate changes

induced by these volcanic eruptions may have been strong enough to affect both high latitude and low latitude climate. These proxies suggest both colder high latitude ocean surface temperature and a southward shift in the ITCZ. Indeed, the Cariaco Basin Ti record shows an interval of reduced Ti counts from 1220 to 1277 (Figure 8D) suggesting a coeval oscillation of the ITCZ. Recent work reconstructing precipitation over the past 300 years in Mesoamerica found further evidence of long-lasting volcanic effects on tropical climate. The authors observed multi-decadal declines in precipitation coinciding with clusters of large volcanic eruptions in the 19th and 20th centuries (Winter et al., 2015).

If more frequent explosive volcanism during the 13th century contributed to a lull in Atlantic hurricane activity, more broadly we might expect to see a lull in activity in other high-resolution reconstructions. The reconstruction from Salt Pond, MA (Donnelly et al., 2015) is generally inactive from the 12th through the 14th century and thus does not provide evidence of a short term lull in activity in the 13th century. Relatively high levels of hurricane activity are inferred from the Mullet Pond reconstruction (Lane et al., 2011) during the mid-12th to the late 13th centuries (Figure 8). Thus, while The Bahamas were seeing a decrease in landfalling storms, regional climate in the Gulf of Mexico was promoting storm survival and growth. Pausata and Camargo (2019) found that large volcanic eruptions can alter the spatial distribution of tropical cyclones on short timescales (~4 years) rather than globally reduce them (Pausata & Camargo, 2019). Some areas experience more storms while others experience less depending on the location of the volcanic cooling and the subsequent volcanically induced displacement of the ITCZ. Perhaps a redistribution of tropical cyclone activity during a particular combination of volcanic eruptions might cause this multi-decadal increase in tropical cyclone activity around the Gulf Coast while also concurrently reducing storm activity in The Bahamas. To assess this hypothesis, we need more modeling work and proxies/multi-proxy approaches to investigating global tropical cyclone distributions on decadal timescales after multiple volcanic eruptions of various sizes and character.

In contrast, other intervals of more frequent explosive volcanism do not appear to correspond to a reduction in event bed frequency at AM4. For example, increased volcanism observed in the 18th and early 19th centuries (Gao et al., 2008) corresponds to an interval of increased hurricane activity on South Andros Island (Figure 8). Recent modeling work suggests that the climate's response to volcanism is dependent on the initial climate conditions (Zanchettin et al., 2019). Zanchettin et al. (2019) found indistinguishable temperature responses in climate simulations for different realistic combinations of volcanic forcing and initial climate states. Hence, one period of time in our record might see a rapid cooling of the environment and subsequent decrease in hurricane activity (e.g., 13th century) while another time period (e.g., 18th century) may not. Overall, the synchronous occurrence of the gap in hurricane activity on South Andros and increased volcanic activity in ice core records during the 13th century suggests that volcanic activity may have contributed to fewer hurricanes in The Bahamas. However, this same relationship does not necessarily apply for every period of high volcanic activity or for all hurricane records in the Atlantic. If explosive volcanism plays a role in modulating hurricane activity, there may be significant spatial variations in those impacts (Pausata & Camargo, 2019). We need more modeling studies that assess how different combinations of large volcanic eruptions with different initial climate states affect large scale climate and the global distribution of tropical cyclones.

The complete record of hurricane activity from South Andros shows greater centennial scale variability than the Mann et al. (2009) basin-wide hindcast of hurricane activity obtained using a statistical model (henceforth referred to as Mann09) (Figure S5). This model drives Atlantic hurricane activity based on proxy reconstructions of the SSTs over the MDR, changes in El Niño Southern Oscillation (ENSO), and the North Atlantic Oscillation (NAO). While both the AM4 and Mann09 records show a peak in activity during the Medieval Warm Period (900–1100 CE) when SSTs were high in the MDR (Figure S5), there is very little other centennial scale variability in the Mann09 record. In particular, the Mann09 hindcast does not show a quiet period of hurricane activity in the mid-13th century when we have suggested increased volcanic activity may have reduced the number of storms in the MDR. A basin-wide estimate like the Mann09 record would smooth out any regional differences in paleohurricane activity. Our comparison of the Mann09 record with our South Andros reconstruction suggests either that a modeled combination of SSTs, ENSO, and NAO cannot capture all of the variability we observe at South Andros Island, or that regional variations in hurricane tracks that show up in a singular record like South Andros cannot be inferred from a smoothed basin-wide estimate like the Mann09 record (Mann et al., 2009).

On the whole, our reconstruction from South Andros suggests relatively few hurricanes over the last 200 years compared to the preceding millennia. Indeed, AM4 only captured two events in the modern era (1850 to present). This relative quiescence is not typical of the record over the last 1500 years and suggests that South Andros may be at higher risk of intense hurricane strikes than implied by the instrumental record. This matches the nearby Blackwood Sinkhole record from Abaco Island (van Hengstum et al., 2016) making it the second record from The Bahamas to show far fewer hurricanes over the observational interval.

4.5. Comparison to Other High-Resolution Hurricane Records

Examining reconstructions from throughout the Atlantic basin helps us to better constrain what inter-regional changes in hurricane activity in the Atlantic were like over the past 1500 years. Comparing AM4 to similarly resolved records from Mullet Pond on the Florida Gulf Coast (Lane et al., 2011) and Salt Pond in Massachusetts (Donnelly et al., 2015), South Andros and Florida activity directly contrast with records from the U.S. East Coast. To test whether transitions from active to inactive or inactive to active are synchronous or time transgressive, we plot the age distributions for the beginnings and ends of some of the more recent active intervals in the Salt Pond, Mullet Pond, and AM4 records (Figure 9). To create our age distributions, we sampled 1000 different age ensembles from our Bayesian age models for Salt Pond, Mullet Pond, and AM4 outputs (Figure 4A and Figure S6). The age models for Salt Pond and Mullet Pond were recreated using BACON software (Blaauw & Christen, 2011) and the 100-year window event frequency in each record was computed (Figure 9). In order to better constrain the age of the transition in hurricane activity at Mullet Pond (Lane et al., 2011), three new radiocarbon dates were added to the previously published chronology and are documented in the supplementary material (Figure S6b and Table S4). By comparing the 100-year event frequency in each of these locations, we capture the centennial scale variations in hurricane strikes at each location and how they compare.

For the first 500 years of the reconstructions (~450–1000 CE), most active intervals in the Mullet Pond High Threshold (HT) and South Andros Island records occur during the same time periods. In contrast, Mullet Pond HT and South Andros activity is not synchronous with Salt Pond activity (Figure 9). Increased hurricane activity at Mullet Pond and on South Andros tends to start just as hurricane activity on Salt Pond ends and vice versa (i.e., Figure 9E). This is true even given the larger uncertainties associated with the Mullet Pond age model (Figure S6b).

For the past millennium, a slightly different pattern emerges. Active intervals at Mullet Pond and South Andros begin at approximately the same time (~1150 CE) within age uncertainties (Figure 9). The Mullet Pond HT record remains active until 1320 CE. Even with 40 years of age uncertainty, this termination of activity is well before Salt Pond's most recent active interval begins in 1420 CE (Figure 9F). Salt Pond experiences increased activity from approximately 1420 to 1675 CE containing ten event beds, with five of these events occurring from 1500 to 1600 CE, an interval that is relatively quiescent at Mullet Pond and South Andros. While South Andros first transitions into higher levels of activity at approximately the same time as Mullet Pond (Figure 9E), it remains active approximately a century after Mullet Pond transitions to lower levels of activity (until ~1470 CE). Its termination is outside of the age distribution of Mullet Pond's termination in activity and occurs after the start of the Salt Pond's active interval (Figure 9E).

The hurricane patterns from the last millennium in Salt Pond and Mullet Pond are confirmed by a variety of lower resolution hurricane proxy records along the U.S. East Coast and Gulf of Mexico. A nearby paleohurricane record from Spring Creek Pond in Apalachee Bay, Florida (Brandon et al., 2013) and a record from a coastal pond in Hancock County, Mississippi (Bregy et al., 2018) confirm the increased hurricane activity from ~1150 to 1350 CE observed at Mullet Pond and South Andros. Both records also indicate quiescence from 1350 CE to present. Along the U.S. East Coast, records from New England (Boldt et al., 2010; Buynevich & Donnelly, 2006; Donnelly et al., 2001; van de Plassche et al., 2006) and the Southeast (Mallinson et al., 2011) show increased storminess during the 15th and 16th centuries. A reconstruction from Mattapoisett Marsh in Massachusetts is the most active from 1400 to 1675 CE with nine overwash deposits identified (Boldt et al., 2010). Other marsh records from southeastern Massachusetts (Buynevich & Donnelly, 2006), Rhode Island (Donnelly et al., 2001), and Connecticut (van de Plassche et al., 2006) show signs of increased storminess during this period including overwash deposits and extensive erosion events.

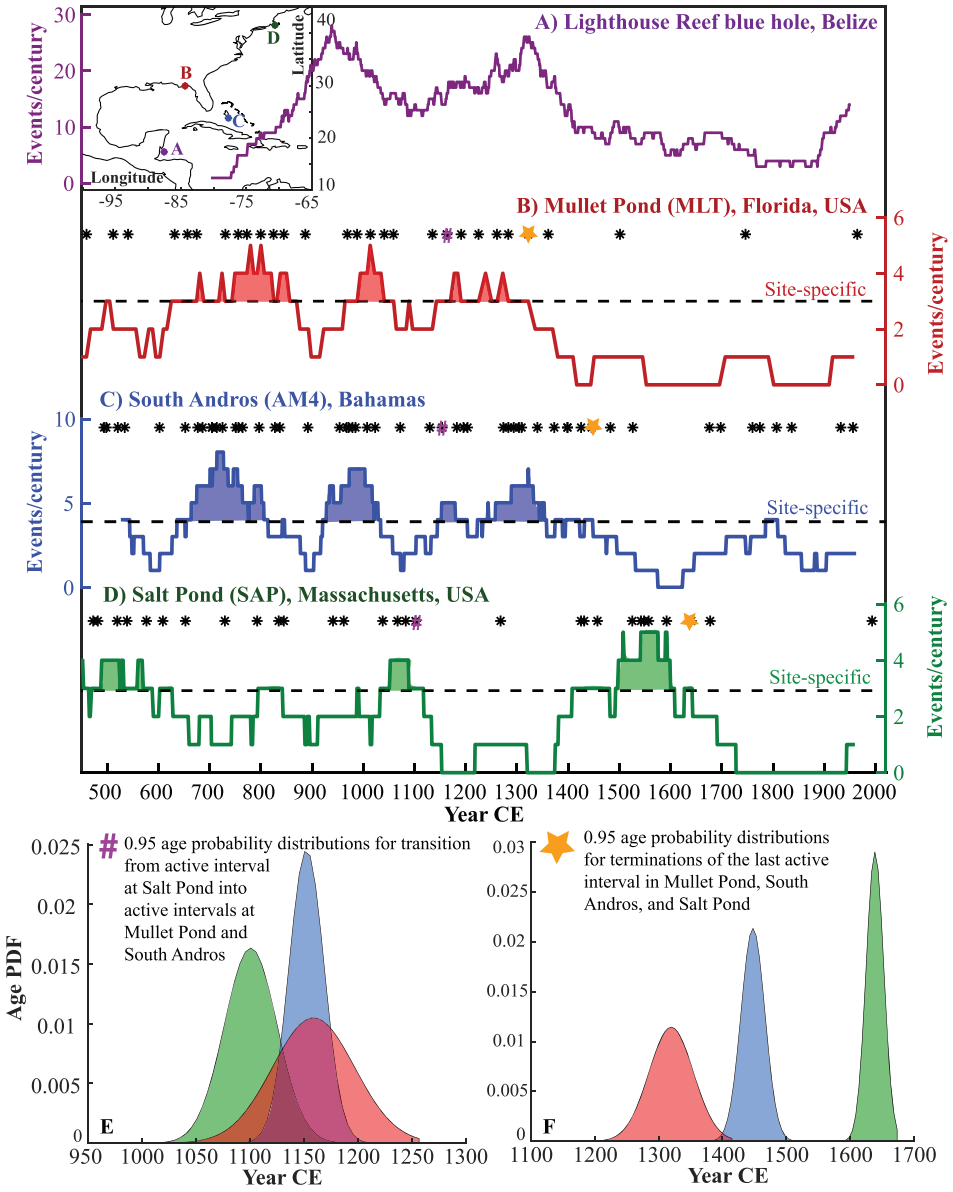

Figure 9. 100-year moving window event frequency on **(A)** Lighthouse Reef Blue Hole, Belize (Denommee et al., 2014) (purple), **(B)** on Mullet Pond, FL (Lane et al., 2011) (red) with 3 active intervals highlighted in red, **(C)** South Andros Island (blue) with the 4 active intervals highlighted in blue, and **(D)** Salt Pond, MA (Donnelly et al., 2015) (green) with 3 active intervals highlighted in green. The timing of each event in the records is denoted by the black stars above each panel. **(E and F)** 95% probability distributions for the transition from an active interval at Salt Pond (green) to active intervals at South Andros (blue) and Mullet Pond (red) ca. 1120 CE and the termination of the last active interval in Salt Pond (green), South Andros (blue), and Mullet Pond (red) ca. 1300–1650 CE. The age probability distributions are calculated around the closest event in the record lying within the active interval. Symbols (pound sign for E, star for F) indicate which events were used for the PDFs**.** Map in the top left corner shows the location of each of the sites.

Moving south, a record of barrier island breaching from the Outer Banks in North Carolina documents fifteen barrier-beach breaches from 1400 to 1675 CE compared to the one to two breaches that occurred in the preceding and following two centuries (Mallinson et al., 2011). Overall, this suggests that coherency observed between our South Andros record and the Mullet Pond record and the disconnect observed between South Andros and Salt Pond applies to the whole Gulf Coast and U.S. East Coast not just western Florida and Massachusetts.

Increased hurricane activity observed during the past millennium at Lighthouse Reef Blue Hole in Belize (Denommee et al., 2014) matches with the Mullet Pond HT reconstruction (Figure 9). Like Mullet Pond, higher levels of activity in Belize end around 1380 CE before activity at Salt Pond increases. Assessing the synchronicity of active intervals across these records suggests three stages of hurricane activity happening over the past millennium: 1) From ~1150 to 1350 CE, there is more hurricane activity in the southern Caribbean Sea and Gulf of Mexico with storms striking Belize and the Gulf Coast (near western Florida) in combination with more storms in the southern Bahamas (near South Andros Island). 2) From ~1350 to 1470 CE, intense hurricane activity is reduced in the southern Caribbean and Gulf of Mexico. We continue to see increased activity in the southern Bahamas and begin to observe increased storm activity along U.S. East Coast. 3) From ~1470 to 1675 CE, intense storms are predominantly making landfall only along the U.S. East Coast.

Two possible reasons arise for why we might observe this transition from activity in the Gulf of Mexico/Caribbean Sea to activity solely along the U.S. East Coast: 1) the local environmental conditions were unfavorable for intense hurricanes to maintain their strength until they reached either the U.S. East Coast or Gulf of Mexico (Kossin, 2017) or 2) variability in storms tracks resulted in more storms veering into one basin over the next (Daloz et al., 2015; Kossin et al., 2010).

Recent research has provided support for both hypotheses. Local environmental conditions can have a significant impact on hurricane genesis and growth. Warmer local SSTs provide more energy for storms, and vertical wind shear prevents hurricanes from reaching their maximum potential intensity (Emanuel, 2003). Indeed, Kossin (2017) investigated environmental conditions along the U.S. East Coast and in the MDR over the last 50 years. He found that when conditions in the MDR were favorable for hurricane formation, vertical wind shear along the U.S. East Coast was anomalously strong and local SSTs were colder. Essentially, in years when the basin-wide activity was elevated, local environmental conditions along the U.S. East Coast were unfavorable for hurricane growth and survival (Kossin, 2017). It is possible that from 1150 to 1400 CE, when activity was low at Salt Pond, such inhibiting conditions were in place along the U.S. East Coast. Alternatively, regional climate can also promote more hurricanes resulting from tropical transition. A subset of storms that impact the U.S. Northeast Coast develop from extratropical disturbances that form in the subtropical western Atlantic in a process known as tropical transition (McTaggart-Cowan et al., 2007). Donnelly et al. (2015) suggested that increased high latitude cooling during the Little Ice Age (1400–1600 CE) shifted the track of extratropical disturbances southward into the subtropical Atlantic facilitating more tropical transitioning hurricanes making landfall at Salt Pond.

Alternatively, many studies have investigated hurricane track variability over decadal timescales to centennial timescales looking at how the position of the North Atlantic Subtropical High (NASH) and Hadley Cell can change the paths of Atlantic hurricanes (Baldini et al., 2016; Elsner, 2003; Elsner & Kocher, 2000; Lucas et al., 2013; Studholme & Gulev, 2018; van Hengstum et al., 2016; Wang et al., 2011; Xie et al., 2005). The strength and position of subtropical ridges across the North Atlantic can modulate hurricane tracks. When the NASH is displaced toward the northeast, there is an increased pressure gradient and strong mid-latitude westerlies that pull warm moist air and consequently, hurricane tracks around the western edge of the high. This causes hurricanes to recurve away from the Gulf of Mexico and instead track towards the U.S. East Coast (Elsner, 2003; McCloskey et al., 2013; Ortegren & Maxwell, 2014). The opposite is true when the subtropical high is positioned more to the southwest. In this case, the subtropical high maintains easterly steering currents, and more hurricanes are characterized as straight-moving and intensify at low latitudes moving through the Caribbean Sea into the Gulf of Mexico (Elsner, 2003; Elsner et al., 2000; Kossin et al., 2010; McCloskey et al., 2013; Ortegren & Maxwell, 2014). The strength of the NASH also plays an important role in determining hurricane track variability. When the NASH is weak and its western ridge erodes, hurricane tracks are more likely to recurve northward moving through the eroded region (Kossin et al., 2010).

At the same time, Hadley Cell position can also impact hurricane genesis and tracks. Recent studies have noted a poleward migration of global tropical cyclone genesis and maximum intensity over the past 30 years connected to poleward Hadley Cell expansion (Kossin et al., 2014; Sharmila & Walsh, 2018; Studholme & Gulev, 2018). This recent Hadley Cell expansion shifts tropical-cyclone-favorable climate conditions poleward in many major ocean basins, in particular by increasing (decreasing) vertical wind shear in the

tropics (subtropics) (Kossin et al., 2014). However, this has not been true for the North Atlantic basin in the last 30 years, in part because of the weak signal for recent Hadley Cell expansion in this basin (Sharmila & Walsh, 2018; Studholme & Gulev, 2018). Despite the current uncertain connection between Hadley Cell expansion and poleward shifting hurricane tracks in the North Atlantic, Baldini et al. (2016) suggests that an expanded Hadley Cell contributed to a northward shifted NASH and thus northward recurving hurricane tracks over the past 500 years using both a new stalagmite record from Belize and documentary records of hurricanes in the Atlantic.

Thus, a second possibility is that from 1150 to 1650 CE we see a gradual shift in hurricane tracks to the northeast through a northward shift in the position of the NASH and/or a weakening of the western ridge of the NASH with an expansion of the Hadley Cell. This would shift storms tracks from straight-moving storms impacting the western Caribbean and Gulf Coast to recurving storms that affect the U.S. East Coast. South Andros Island serves as a transitional point for this shift in tracks staying active for most of the time period when storms are hitting the Gulf Coast and remaining active as tracks shift northeastward out of the Gulf of Mexico to up along the U.S. East Coast. More high-resolution paleohurricane reconstructions from throughout the Caribbean and Gulf of Mexico are necessary to determine whether this disconnect between Gulf of Mexico/Bahamas records and U.S. East Coast records is a result of changes in local environmental conditions (e.g., SSTs, thermocline depth), regional variability in hurricane tracks, or some combination of both mechanisms.

5. Conclusions

This study presents a near annually resolved record of intense hurricane activity derived from three blue holes positioned in the carbonate tidal flats on South Andros Island in The Bahamas. The reconstruction is the longest high resolution Caribbean paleohurricane record spanning the past 1500 years. We found that coarse-grained sediment layers in the stratigraphy during the historic period corresponded to the passage of intense hurricane events (category 3 or above) within 50 km of the site. Sediment records from all three blue holes on the island showed similar patterns of hurricane deposition, despite their different geomorphologic position and orientation.

This study exemplifies the importance of looking to long-term proxy records to make hurricane risk assessments for a particular area. It is clear from this work that historical records of hurricane activity underestimate hurricane landfall recurrence rate at South Andros. In the last 70 years, there has not been a single intense hurricane passing close enough to South Andros to leave an event deposit. There is a 10% probability of having such a gap in activity given the recurrence interval of storms over the past 1500 years.

The frequency of intense hurricane landfalls on South Andros Island has varied dramatically over the past 1500 years. In particular, we document four multi-decadal periods when hurricane activity on South Andros has significantly exceeded historical levels (640–815 CE, 920–1035 CE, 1145–1205 CE, and 1300–1450 CE). Three of these active intervals correspond to time periods when the ITCZ was farther northward (Haug et al., 2001), which suggests that the ITCZ position plays a role in determining hurricane activity that affects the island. However, the first active interval in the record corresponds to a neutral to southerly ITCZ position, suggesting that other factors were at play during this period of activity. An anomalous quiet period on South Andros in the early 13th century may point to volcanic activity contributing to changes in Atlantic hurricane activity. However, the hurricane response to volcanos differs from region to region and may be dependent on initial climate conditions.

The timing of active intervals over the past millennium (~1100–2015 CE) of the record suggests that hurricane active (inactive) intervals at South Andros occur simultaneously with increased (decreased) landfalls in a Gulf of Mexico record and a record from Belize. In contrast, records from the U.S. East Coast show increased hurricane activity when South Andros is relatively quiet. We suggest a gradual shift in hurricane tracks to the northeast over the past millennium. Straight-moving storms hitting the western Caribbean and Gulf Coast transform into recurving storms that affect the U.S. East Coast. This could be a result of decadal variability in hurricane tracks related to variations in the mean position and strength of the North Atlantic Subtropical High and/or changes in local environmental factors. More high-resolution paleohurricane reconstructions from throughout the Caribbean and Gulf of Mexico are necessary to better constrain how storm activity shifted from lower latitudes to the U.S. East Coast.

Acknowledgments

This work was funded by the National Science Foundation Graduate Research Fellowship (to E.J.W.), National Science Foundation grant OCE-1356708 (to J.P.D. and P.J.vH.), the Dalio Explore Foundation and the USGS Land Change Science Program (M.R.T.). We are grateful to members of WHOI Coastal Systems Group, in particular Stephanie Madsen, for their help in the processing core samples. We thank two anonymous reviewers, Matthew Lachniet, Marci Robinson (USGS) and Miriam Jones (USGS) for their helpful feedback on earlier versions of this manuscript. Any use of trade, firm, or product names is for descriptive purposes only and does not imply endorsement by the U.S. Government. The data are available on the National Climatic Data Center (http://www.ncdc.noaa.gov/dataaccess/paleoclimatology-data) and WHOI Coastal Systems Group (https://web.whoi.edu/coastal-group/) websites.

References

Baldini, L. M., Baldini, J. U. L., McElwaine, J. N., Frappier, A. B., Asmerom, Y., Liu, K., et al. (2016). Persistent northward North Atlantic tropical cyclone track migration over the past five centuries. *Scientific Reports*, *6*(1). https://doi.org/10.1038/srep37522

Blaauw, M., & Christen, J. A. (2011). Flexible paleoclimate age-depth models using an autoregressive gamma process. *Bayesian Analysis*, *6*(3), 457–474. https://doi.org/10.1214/11-BA618

Black, M. (1933). The Algal Sediments of Andros Island, Bahamas. *Philosophical Transactions of the Royal Society of London*, *222*(B), 165–192.

Boardman, M. R., & Neumann, A. C. (1984). Sources of periplatform carbonates: Northwest Providence Channel, Bahamas. *Journal of Sedimentary Petrology*, *54*(4), 1110–1123.

Boldt, K. V., Lane, P., Woodruff, J. D., & Donnelly, J. P. (2010). Calibrating a sedimentary record of overwash from Southeastern New England using modeled historic hurricane surges. *Marine Geology*, *275*(1–4), 127–139. https://doi.org/10.1016/j.margeo.2010.05.002

Bourrouilh-le Jan, F. G. (2007). Very high energy sedimentation (supratidal hurricane deposits) and Mid-Holocene highstand on carbonate platforms, Andros, Bahamas: An alternative view. *Sedimentary Geology*, *199*, 29–49. https://doi.org/10.1016/j.sedgeo.2005.12.032

Brandon, C. M., Woodruff, J. D., Lane, D. P., & Donnelly, J. P. (2013). Tropical cyclone wind speed constraints from resultant storm surge deposition: A 2500 year reconstruction of hurricane activity from St. Marks, FL. *Geochemistry, Geophysics, Geosystems*, *14*, 2993–3008. https://doi.org/10.1002/ggge.20217

Bregy, J. C., Wallace, D. J., Totten, R., & Cruz, V. J. (2018). 2500-year paleotempestological record of intense storms for the northern Gulf of Mexico, United States. *Marine Geology*, *396*, 26–42. https://doi.org/10.1016/j.margeo.2017.09.009

Brown, A. L., Reinhardt, E. G., van Hengstum, P. J., & Pilarczyk, J. E. (2014). A Coastal Yucatan Sinkhole Records Intense Hurricane Events. *Journal of Coastal Research*, *30*(2), 418–429. https://doi.org/10.2112/JCOASTRES-D-13-00069.1

Buynevich, I. V., & Donnelly, J. P. (2006). Geological Signatures of Barrier Breaching and Overwash, Southern Massachusetts, USA. *Journal of Coastal Research*, *1*(39), 112–116.

Carew, J. L., Mylroie, J. E., & Schwabe, S. J. (1998). The geology of South Andros Island, Bahamas: A reconnaissance report. *Cave and Karst Science*, *25*(2), 57–66.

Church, J. A., White, N. J., & Arblaster, J. M. (2005). Significant decadal-scale impact of volcanic eruptions on sea level and ocean heat content. *Nature*, *438*(7064), 74–77. https://doi.org/10.1038/nature04237

Daloz, A. S., Camargo, S. J., Kossin, J. P., Emanuel, K., Horn, M., Jonas, J. A., et al. (2015). Cluster Analysis of Downscaled and Explicitly Simulated North Atlantic Tropical Cyclone Tracks. *Journal of Climate*, *28*(4), 1333–1361. https://doi.org/10.1175/JCLI-D-13-00646.1

Denommee, K. C., Bentley, S. J., & Droxler, A. W. (2014). Climatic controls on hurricane patterns: a 1200-y near-annual record from Lighthouse Reef Belize. *Scientific Reports*, *4*(1). https://doi.org/10.1038/srep03876

Dill, R. F. (1977). The blue holes - Geologically significant submerged sink holes and caves off British Honduras and Andros, Bahama Islands. *Proceedings of Third International Coral Reef Symposium*, *2*, 237–242.

Donnelly, J. P., Hawkes, A. D., Lane, P., MacDonald, D., Shuman, B. N., Toomey, M. R., et al. (2015). Climate forcing of unprecedented intense-hurricane activity in the last 2000 years. *Earth's Future*, *3*(2), 49–65. https://doi.org/10.1002/2014EF000274

Donnelly, J. P., Smith Bryant, S., Butler, J., Dowling, J., Fan, L., Hausmann, N., et al. (2001). 700 yr sedimentary record of intense hurricane landfalls in southern New England. *Geological Society of America Bulletin*, *113*(6), 714–727. https://doi.org/10.1130/0016-7606(2001)113<0714:YSROIH>2.0.CO;2

Donnelly, J. P., & Woodruff, J. D. (2007). Intense hurricane activity over the past 5,000 years controlled by El Niño and the West African monsoon. *Nature*, *447*(7143), 465–468. https://doi.org/10.1038/nature05834

Elsner, J. B. (2003). Tracking hurricanes. *Bulletin of the American Meteorological Society*, *84*(3), 353–356. https://doi.org/10.1175/BAMS-84-3-353

Elsner, J. B., Liu, K., & Kocher, B. (2000). Spatial variations in major U.S. hurricane activity: Statistics and a physical mechanism. *Journal of Climate*, *13*, 2293–2305. https://doi.org/10.1175/1520-0442(2000)013<2293:SVIMUS>2.0.CO;2

Elsner, J. B., & Kocher, B. (2000). Global Tropical Cyclone Activity: A Link to the North Atlantic Oscillation. *Journal of Geophysical Research*, *27*(1), 129–132. https://doi.org/10.1029/1999GL010893

Emanuel, K. (2003). Tropical Cyclones. *Annual Review of Earth and Planetary Sciences*, *31*(1), 75–104. https://doi.org/10.1146/annurev.earth.31.100901.141259

Evan, A. T. (2012). Atlantic hurricane activity following two major volcanic eruptions. *Journal of Geophysical Research*, *117*, D06101. https://doi.org/10.1029/2011JD016716

Fairbanks, R. G. (1989). A 17,000-year glacio-eustatic sea level record: influence of glacial melting rates on the Younger Dryas event and deep-ocean circulation. *Nature*, *342*(6250), 637–642. https://doi.org/10.1038/342637a0

Frappier, A., Knutson, T., Liu, K. B., & Emanuel, K. (2007). Perspective: Coordinating paleoclimate research on tropical cyclones with hurricane-climate theory and modelling. *Tellus, Series A: Dynamic Meteorology and Oceanography*, *59*(4), 529–537. https://doi.org/10.1111/j.1600-0870.2007.00250.x

Gao, C., Robock, A., & Ammann, C. (2008). Volcanic forcing of climate over the past 1500 years: An improved ice core-based index for climate models. *Journal of Geophysical Research*, *113*, D16112. https://doi.org/10.1029/2008JD010239

Gischler, E., Anselmetti, F. S., & Shinn, E. A. (2013). Seismic stratigraphy of the Blue Hole (Lighthouse Reef, Belize), a late Holocene climate and storm archive. *Marine Geology*, *344*, 155–162. https://doi.org/10.1016/j.margeo.2013.07.013

Gischler, E., Shinn, E. A., Oschmann, W., Fiebig, J., & Buster, N. A. (2008). A 1500-Year Holocene Caribbean Climate Archive from the Blue Hole, Lighthouse Reef, Belize. *Journal of Coastal Research*, *246*(246), 1495–1505. https://doi.org/10.2112/07-0891.1

Gray, W. M. (1998). The Formation of Tropical Cyclones. *Meteorology and Atmospheric Physics*, *67*, 37–69. https://doi.org/10.1007/BF01277501

Gregory, B. R. B., Reinhardt, E. G., & Gifford, J. A. (2017). The Influence of Morphology on Sinkhole Sedimentation at Little Salt Spring, Florida. *Journal of Coastal Research*, *33*(2), 359–372. https://doi.org/10.2112/JCOASTRES-D-15-00169.1

Hansen, J., Sato, M., Ruedy, R., Nazarenko, L., Lacis, A., Schmidt, G. A., et al. (2005). Efficacy of climate forcings. *Journal of Geophysical Research*, *110*, D18104. https://doi.org/10.1029/2005JD005776

Haug, G. H., Hughen, K. A., Sigman, D. M., Peterson, L. C., Röhl, U., Peterson, L. C., et al. (2001). Southward migration of the intertropical convergence zone through the Holocene. *Science (New York, N.Y.)*, *293*(5533), 1304–1308. https://doi.org/10.1126/science.1059725

Hua, Q., Barbetti, M., & Rakowski, A. (2013). Atmospheric radiocarbon for the period 1950–2010. *Radiocarbon*, *55*(4), 2059–2072.

Hubbard, D. K., Zankl, H., Van Heerden, I., & Gill, I. P. (2005). Holocene Reef Development Along the Northeastern St. Croix Shelf, Buck Island, U.S. Virgin Islands. *Journal of Sedimentary Research*, *75*(1), 97–113. https://doi.org/10.2110/jsr.2005.009

Juberthie, C., & Iliffe, T. M. (1994). Bahama Islands. *Encyclopaedia Biospeologica*, 449–458.

Khan, N. S., Ashe, E., Horton, B. P., Dutton, A., Kopp, R. E., Brocard, G., et al. (2017). Drivers of Holocene sea-level change in the Caribbean. *Quaternary Science Reviews*, *155*, 13–36. https://doi.org/10.1016/j.quascirev.2016.08.032

Kier, J. S., & Pilkey, O. H. (1971). The influence of sea level changes on sediment carbonate mineralogy, Tongue of the Ocean, Bahamas. *Marine Geology*, *11*, 189–200.

Kishore, N., Marqués, D., Mahmud, A., Kiang, M. V., Rodriguez, I., Fuller, A., et al. (2018). Mortality in Puerto Rico after Hurricane Maria. *The New England Journal of Medicine*, *379*(2), 162–170. https://doi.org/10.1056/NEJMsa1803972

Korty, R. L., Camargo, S. J., & Galewsky, J. (2012). Variations in tropical cyclone genesis factors in simulations of the Holocene epoch. *Journal of Climate*, *25*(23), 8196–8211. https://doi.org/10.1175/JCLI-D-12-00033.1

Kossin, J. P. (2017). Hurricane intensification along United States coast suppressed during active hurricane periods. *Nature*, *541*(7637), 390–393. https://doi.org/10.1038/nature20783

Kossin, J. P., Camargo, S. J., & Sitkowski, M. (2010). Climate modulation of North Atlantic hurricane tracks. *Journal of Climate*, *23*(11), 3057–3076. https://doi.org/10.1175/2010JCLI3497.1

Kossin, J. P., Emanuel, K. A., & Vecchi, G. A. (2014). The poleward migration of the location of tropical cyclone maximum intensity. *Nature*, *509*(7500), 349–352. https://doi.org/10.1038/nature13278

Kossin, J. P., & Vimont, D. J. (2007). A more general framework for understanding atlantic hurricane variability and trends. *Bulletin of the American Meteorological Society*, *88*(11), 1767–1781. https://doi.org/10.1175/BAMS-88-11-1767

Landsea, C. W., & Franklin, J. L. (2013). Atlantic Hurricane Database Uncertainty and Presentation of a New Database Format. *Monthly Weather Review*, *141*(10), 3576–3592. https://doi.org/10.1175/MWR-D-12-00254.1

Lane, P., & Donnelly, J. P. (2012). Hurricanes and Typhoons - Will tropical cyclones become stronger and more frequent? *Past. PAGES News*, *20*(1), 33.

Lane, P., Donnelly, J. P., Woodruff, J. D., & Hawkes, A. D. (2011). A decadally-resolved paleohurricane record archived in the late Holocene sediments of a Florida sinkhole. *Marine Geology*, *287*(1–4), 14–30. https://doi.org/10.1016/j.margeo.2011.07.001

Lin, N., Lane, P., Emanuel, K. A., Sullivan, R. M., & Donnelly, J. P. (2014). Heightened hurricane surge risk in northwest Florida revealed from climatological-hydrodynamic modeling and paleorecord reconstruction. *Journal of Geophysical Research: Atmospheres*, *119*, 8606–8623. https://doi.org/10.1002/2014JD021584

Liu, K., & Fearn, M. L. (1993). Lake-sediment record of late Holocene hurricane. *Geology*, *21*(September), 793–796. https://doi.org/10.1130/0091-7613(1993)021<0793

Lucas, C., Timbal, B., & Nguyen, H. (2013). The expanding tropics: A critical assessment of the observational and modeling studies. *Wiley Interdisciplinary Reviews: Climate Change*, *5*(1), 89–112. https://doi.org/10.1002/wcc.251

Maiklem, W. R. (1968). Some hydraulic properties of bioclastic carbonate grains. *Sedimentology*, *10*, 101–109.

Mallinson, D. J., Smith, C. W., Mahan, S., Culver, S. J., & McDowell, K. (2011). Barrier island response to late Holocene climate events, North Carolina, USA. *Quaternary Research*, *76*(1), 46–57. https://doi.org/10.1016/j.yqres.2011.05.001

Maloof, A. C., & Grotzinger, J. P. (2012). The Holocene shallowing-upward parasequence of north-west Andros Island, Bahamas. *Sedimentology*, *59*, 1375–1407. https://doi.org/10.1111/j.1365-3091.2011.01313.x

Mann, M. E., Bradley, R. S., & Hughes, M. K. (1999). Northern Hemisphere Temperatures During the Past Millennium: Inferences, Uncertainties, and Limitations. *Geophysical Research Letters*, *26*(6), 759–762.

Mann, M. E., Woodruff, J. D., Donnelly, J. P., & Zhang, Z. (2009). Atlantic hurricanes and climate over the past 1,500 years. *Nature*, *460*(7257), 880–883. https://doi.org/10.1038/nature08219

McCloskey, T., Bianchette, T., & Liu, K. (2013). Track Patterns of Landfalling and Coastal Tropical Cyclones in the Atlantic Basin, Their Relationship with the North Atlantic Oscillation (NAO), and the Potential Effect of Global Warming. *American Journal of Climate*, *2*, 12–22. https://doi.org/10.4236/ajcc.2013.23A002

Mckee, K. L., Cahoon, D. R., & Feller, I. C. (2007). Caribbean mangroves adjust to rising sea level through biotic controls on change in soil elevation. *Global Ecology and Biogeography*, *16*(5), 545–556. https://doi.org/10.1111/j.1466-8238.2007.00317.x

McTaggart-Cowan, R., Deane, G. D., Bosart, L. F., Davis, C. A., & Galarneau, T. J. (2007). Climatology of Tropical Cyclogenesis in the North Atlantic (1948 –2004). *Monthly Weather Review*, *136*, 1284–1304. https://doi.org/10.1175/2007MWR2245.1

Miller, M. C., McCave, I. N., & Komar, P. D. (1977). Threshold of sediment motion under unidirectional currents. *Sedimentology*, *24*(4), 507–527. https://doi.org/10.1111/j.1365-3091.1977.tb00136.x

Milliman, J. D., Freile, D., Steinen, R. P., & Wilber, R. J. (1993). Great Bahama Bank Aragonitic Muds: Mostly Inorganically Precipitated, Mostly Exported. *Journal of Sedimentary Petrology*, *63*(4), 589–595.

Milne, G. A., & Peros, M. (2013). Data-model comparison of Holocene sea-level change in the circum-Caribbean region. *Global and Planetary Change*, *107*, 119–131. https://doi.org/10.1016/j.gloplacha.2013.04.014

Mullins, H. T., & Lynts, G. W. (1977). Origin of the northwestern Bahama Platform: Review and reinterpretation. *Geological Society of America Bulletin*, *88*, 1447–1461.

Mylroie, J. E., Carew, J. L., & Moore, A. I. (1995). Blue holes: Definition and genesis. *Carbonates and Evaporites*, *10*(2), 225–233. https://doi.org/10.1007/BF03175407

Ortegren, J. T., & Maxwell, J. T. (2014). Spatiotemporal Patterns of Drought/Tropical Cyclone Co-occurrence in the Southeastern USA: Linkages to North Atlantic Climate Variability. *Geography Compass*, *8*, 540–559.

Otvos, E. G. (2011). Hurricane signatures and landforms-toward improved interpretations and global storm climate chronology. *Sedimentary Geology*, *239*(1–2), 10–22. https://doi.org/10.1016/j.sedgeo.2011.04.014

Pausata, F. S. R., & Camargo, S. J. (2019). Tropical cyclone activity affected by volcanically induced ITCZ shifts. *Proceedings of the National Academy of Sciences*, *116*(16), 7732–7737. https://doi.org/10.1073/pnas.1900777116

Peltier, W. R., & Fairbanks, R. G. (2006). Global glacial ice volume and Last Glacial Maximum duration from an extended Barbados sea level record. *Quaternary Science Reviews*, *25*(23–24), 3322–3337. https://doi.org/10.1016/j.quascirev.2006.04.010

Pilskaln, C. H., Neumann, A. C., & Bane, J. M. (1989). Periplatform carbonate flux in the northern Bahamas. *Deep-Sea Research*, *36*(9), 1391–1406.

Ramcharan, E. K., & McAndrews, J. H. (2006). Holocene Development of Coastal Wetland at Maracas Bay, Trinidad, West Indies. *Journal of Coastal Research*, *223*, 581–586. https://doi.org/10.2112/04A-0001.1

Rankey, E. C., Enos, P., Steffen, K., & Druke, D. (2004). Lack of Impact of Hurricane Michelle on Tidal Flats, Andros Island, Bahamas: Integrated Remote Sensing and Field Observations. *Journal of Sedimentary Research*, *74*(5), 654–661.

Reimer, P. J., Bard, E., Bayliss, A., Beck, J. W., Blackwell, P. G., Ramsey, C. B., et al. (2013). IntCal13 and Marine13 Radiocarbon Age Calibration Curves 0–50,000 Years cal BP. *Radiocarbon*, *55*(4), 1869–1887. https://doi.org/10.2458/azu_js_rc.55.16947

Richey, J. N., Poore, R. Z., Flower, B. P., Quinn, T. M., & Hollander, D. J. (2009). Regionally coherent Little Ice Age cooling in the Atlantic Warm Pool. *Geophysical Research Letters*, *36*, L21703. https://doi.org/10.1029/2009GL040445

Schneider, T., Bischoff, T., & Haug, G. H. (2014). Migrations and dynamics of the intertropical convergence zone. *Nature*, *513*(7516), 45–53. https://doi.org/10.1038/nature13636

Sharmila, S., & Walsh, K. J. E. (2018). Recent poleward shift of tropical cyclone formation linked to Hadley cell expansion. *Nature Climate Change*, *8*(8), 730–736. https://doi.org/10.1038/s41558-018-0227-5

Shinn, E. A., Lloyd, R. M., & Ginsburg, R. N. (1969). Anatomy of Modern Carbonate Tidal Flat, Andros Island, Bahamas. *Journal of Sedimentary Petrology*, *39*(3), 1202–1228.

Shinn, E. A., Reich, C. D., Locker, S. D., & Hine, A. C. (1996). A Giant Sediment Trap in the Florida Keys. *Journal of Coastal Research*, *12*(4), 953–959.

Shinn, E. A., Steinen, R. P., Dill, R. F., & Major, R. (1993). Lime-mud layers in high-energy tidal channels: A record of hurricane deposition. *Geology*, *21*, 603–606.

Sicre, M.-A., Yiou, P., Dahhaoui, I., Knudsen, K., Jansen, E., & Turon, J. (2008). A 4500-year reconstruction of sea surface temperature variability at decadal time-scales off North Iceland. *Quaternary Science Reviews*, *27*, 2041–2047. https://doi.org/10.1016/j.quascirev.2008.08.009

Sigl, M., McConnell, J. R., Toohey, M., Curran, M., Das, S. B., Edwards, R., et al. (2014). Insights from Antarctica on volcanic forcing during the Common Era. *Nature Climate Change*, *4*(8), 693–697. https://doi.org/10.1038/nclimate2293

Spencer, M. (1967). Bahamas Deep Test. *Bulletin of the American Association of Petroleum Geologists*, *51*(2), 263–268.

Studholme, J., & Gulev, S. (2018). Concurrent changes to hadley circulation and the meridional distribution of tropical cyclones. *Journal of Climate*, *31*(11), 4367–4389. https://doi.org/10.1175/JCLI-D-17-0852.1

The hurricane season 2017: a cluster of extreme storms. (n.d.). Retrieved November 10, 2018, from https://www.munichre.com/topics-online/en/climate-change-and-natural-disasters/natural-disasters/storms/hurricane-season-2017.html

Toomey, M. R., Curry, W. B., Donnelly, J. P., & van Hengstum, P. J. (2013). Reconstructing 7000 years of North Atlantic hurricane variability using deep-sea sediment cores from the western Great Bahama Bank. *Paleoceanography*, *28*, 31–41. https://doi.org/10.1002/palo.20012

Toscano, M. A., & Macintyre, I. G. (2003). Corrected western Atlantic sea-level curve for the last 11,000 years based on calibrated 14C dates from Acropora palmata framework and intertidal mangrove peat. *Coral Reefs*, *22*(3), 257–270. https://doi.org/10.1007/s00338-003-0315-4

Ulm, K. (1990). A simple method to calculate the confidence interval of a standardized mortality ratio (SMR). *American Journal of Epidemiology*, *131*(2), 373–375. https://doi.org/10.1093/oxfordjournals.aje.a115507

van Hengstum, P. J., Donnelly, J. P., Fall, P. L., Toomey, M. R., Albury, N. A., & Kakuk, B. (2016). The intertropical convergence zone modulates intense hurricane strikes on the western North Atlantic margin. *Scientific Reports*, *6*(October 2015), 21728. https://doi.org/10.1038/srep21728

van Hengstum, P. J., Donnelly, J. P., Toomey, M. R., Albury, N. A., Lane, P., & Kakuk, B. (2014). Heightened hurricane activity on the Little Bahama Bank from 1350 to 1650 AD. *Continental Shelf Research*, *86*, 103–115. https://doi.org/10.1016/j.csr.2013.04.032

van de Plassche, O., Erkens, G., van Vliet, F., Brandsma, J., van der Borg, K., & de Jong, A. F. M. (2006). Salt-marsh erosion associated with hurricane landfall in southern New England in the fifteenth and seventeenth centuries. *Geology*, *34*(10), 829–832. https://doi.org/10.1130/G22598.1

Wallace, D. J., Woodruff, J. D., Anderson, J. B., & Donnelly, J. P. (2014). Palaeohurricane reconstructions from sedimentary archives along the Gulf of Mexico, Caribbean Sea and western North Atlantic Ocean margins. *Sedimentary Coastal Zones from High to Low Latitudes: Similarities and Differences*, *388*, 481–501. https://doi.org/10.1144/SP388.12

Wang, C., Liu, H., Lee, S. K., & Atlas, R. (2011). Impact of the Atlantic warm pool on United States landfalling hurricanes. *Geophysical Research Letters*, *38*, L19702. https://doi.org/10.1029/2011GL049265

Wilber, R. J., Milliman, J. D., & Halley, R. B. (1990). Accumulation of bank-top sediment on the western slope of Great Bahama Bank: Rapid progradation of a carbonate megabank. *Geology*, *18*(10), 970–974. https://doi.org/10.1130/0091-7613(1990)018<0970:AOBTSO>2.3.CO;2

Winter, A., Zanchettin, D., Miller, T., Kushnir, Y., Black, D., Lohmann, G., et al. (2015). Persistent drying in the tropics linked to natural forcing. *Nature Communications*, *6*(1), 1–8. https://doi.org/10.1038/ncomms8627

Woodruff, J. D., Donnelly, J. P., Emanuel, K., & Lane, P. (2008). Assessing sedimentary records of paleohurricane activity using modeled hurricane climatology. *Geochemistry, Geophysics, Geosystems*, *9*, Q09V10. https://doi.org/10.1029/2008GC002043

Xie, L., Yan, T., Pietrafesa, L. J., Morrison, J. M., & Karl, T. (2005). Climatology and interannual variability of North Atlantic hurricane tracks. *Journal of Climate*, *18*(24), 5370–5381. https://doi.org/10.1175/JCLI3560.1

Zanchettin, D., Timmreck, C., Toohey, M., Jungclaus, J. H., Bittner, M., Lorenz, S. J., & Rubino, A. (2019). Clarifying thfe relative role of forcing uncertainties and initial-condition unknowns in spreading the climate response to volcanic eruptions. *Geophysical Research Letters*, *46*, 1602–1611. https://doi.org/10.1029/2018GL081018

Reference From the Supporting Information

Hsu, S. A., & Yan, Z. (1998). A Note on the Radius of Maximum Wind for Hurricanes. *Journal of Coastal Research*, *14*(2), 667–668.